aerospace

MDPI

Review

A Review of Working Fluids and Flow State Effects on Thermal Performance of Micro-Channel Oscillating Heat Pipe for Aerospace Heat Dissipation

Xiaohuan Zhao [1], Limin Su [1], Jiang Jiang [1], Wenyu Deng [1] and Dan Zhao [2,*]

[1] Energy and Electricity Research Center, International Energy College, Zhuhai Campus, Jinan University, Zhuhai 519070, China
[2] Department of Mechanical Engineering, University of Canterbury, Private Bag 4800, Christchurch 8140, New Zealand
* Correspondence: dan.zhao@canterbury.ac.nz

Abstract: A MCOHP (micro-channel oscillating heat pipe) can provide lightweight and efficient temperature control capabilities for aerospace spacecraft with a high power and small size. The research about the heat flow effects on the thermal performance of MCOHPs is both necessary and essential for aerospace heat dissipation. In this paper, the heat flow effects on the thermal performance of MCOHPs are summarized and studied. The flow thermal performance enhancement changes of MCOHPs are given, which are caused by the heat flow work fluids of nano-fluids, gases, single liquids, mixed liquids, surfactants, and self-humidifying fluids. The use of graphene nano-fluids as the heat flow work medium can reduce the thermal resistance by 83.6%, which can enhance the maximum thermal conductivity by 105%. The influences of gravity and flow characteristics are also discussed. The heat flow pattern changes with the work stage, which affects the flow mode and the heat and mass transfer efficiency of OHP. The effective thermal conductivity varies from 4.8 kW/(m·K) to 70 kW/(m·K) when different gases are selected as the working fluid in OHP. The study of heat flow effects on the thermal performance of MCOHPs is conducive to exploring in-depth aerospace applications.

Keywords: aerospace heat dissipation; micro-channel oscillating heat pipe; heat flow; thermal performance; heat flow pattern

Citation: Zhao, X.; Su, L.; Jiang, J.; Deng, W.; Zhao, D. A Review of Working Fluids and Flow State Effects on Thermal Performance of Micro-Channel Oscillating Heat Pipe for Aerospace Heat Dissipation. *Aerospace* **2023**, *10*, 179. https://doi.org/10.3390/aerospace10020179

Academic Editors: Tiegang Fang and Phil Ligrani

Received: 29 November 2022
Revised: 7 February 2023
Accepted: 9 February 2023
Published: 14 February 2023

1. Introduction

The working environment of aerospace equipment is special, including cold and heat exchange [1,2], heat transfer [3,4], energy mode conversion [5,6], and energy management [7,8]. The heat dissipation that is caused by heat conduction [9,10], heat convection [11,12], and radiation [13,14] during the operation of aerospace equipment should not be underestimated. Oscillating heat pipe (OHP) is the preferred heat dissipation technology for aerospace equipment, battery, and electronic equipment, due to its superior heat transfer performance, simple structure, and miniaturization [15,16]. The changes of the array layout, heating mode, working fluid, pipe wall material, and working fluid flow in the pipe are the primary factors that affect the OHP heat transfer performance [17]. The OHP has been studied using a variety of working fluids and nano-fluids have emerged as a research fad [18]. OHPs with a 3D structure have been mentioned in recent years [19], which can provide excellent performance in some space heat transfer scenarios [20]. The OHP turns [21], and the heating settings and pulsing heating techniques also have an impact on the thermal performance [22,23].

Based on the outcomes of the visualization, Senjaya et al. [24] developed a model for the creation and expansion of tube diameter bubbles. The liquid slug velocity was less than 0.2 m/s, which promotes bubbles formation. Ando et al. [25] tested the OHP with a check valve, which is located near the condensation section. The valve intermittently supplied liquid plugs to the evaporation section to start the pipe successfully. Wang et al. [26] investigated the intricate hydrodynamic processes and presented a new, closed OHP with periodic expansion and contraction condensation. The thermal efficiency was raised by 45% and the contraction condensation increased the oscillation frequency of the vapor plug/liquid slug. Shi et al. [27] performed an experiment investigation on a closed-loop OHP with a 0.5% mass-concentrated micro-encapsulated phase change material suspension. The vertical installation performed better for heat transfer under the effect of gravity. Lim et al. [28] adopted a randomly arranged pipeline layout OHP and studied the internal working fluid oscillation. The liquid slugs oscillated with large amplitude in every channel and the thermal performance was 32% higher than MCOHPs with a uniform channel layout. Liu et al. [29] made 15 turns of the anti-gravity OHP and carried out the research with the heat recovery rate of 1.66 times than that of pure copper tubes, which proved that gravity had a positive effect on the internal hydrodynamics.

The heat transmission capabilities of liquid metal and water as the working fluids of OHPs were compared by Hao et al. [30]. The heat transfer performance of the OHP is increased by 13% when the liquid metal is the working fluid instead of pure water. Schwarz et al. [31] proposed two design methods of floral OHP and star-shaped OHP and conducted experiments. The floral OHP increased the latent heat transfer, while the star-shaped OHP improved the convective heat transfer. The floral OHP design reduced the thermal resistance by 7% in the horizontal position and 12% in the vertical position. Kwon et al. [32] reported the influence of double-diameter tubes on single-turn OHPs. The circular flow was promoted by double-diameter tubes, which reduced the thermal resistance of the OHP by 45%. Liu et al. [33] designed and manufactured a new type of flat-plate OHP (FPOHP) with double serpentine channels. FPOHPs can successfully start at all tilt angles from 0° to 90°. The thermal conductivity of FPOHPs is 5.8 times than that of ordinary OHPs. Arai et al. [34] designed three kinds of polycarbonate OHPs of actual flow channel structures with an additive manufacture method and conducted research. By comparison of the effective thermal conductivity of different flow channel sizes at the same filling ratio, the effective thermal conductivity of a 0.8 mm square flow channel was about seven times that of a 2 mm square flow channel.

The working fluids and flow state have effects on the thermal performance of the micro-channel oscillating heat pipe, which are confirmed by all the above studies. In this paper, the effects of working fluids and the flow state on OHPs factors on the heat transfer performance are studied. The heat dissipation mechanism and technical characteristics of OHP are introduced. The effects of various filling working fluids including metal nano-fluids, filling working fluids, non-metallic nano-fluids, mixed nano-fluids, gas, organic solvents, mixed liquids, surfactants, and self-rewetting fluids (SRWFs) on heat dissipation are listed in detail. The influence of gravity on the flow, the flow pattern characteristics, and the two-phase oscillating flow are compared.

2. Heat Dissipation Mechanism and Characteristics of the MCOHP

2.1. Heat Dissipation Mechanism of the OHP

The working fluid is filled into a vacuum pipe with a certain proportion, which can be blended into various shapes and divided into an evaporation section, adiabatic section, and a condensation section [35]. The working fluid absorbs heat in the evaporation section and releases heat in the condensation section, which can transfer the heat generated at the evaporation section to the condensation section to achieve heat dissipation [36]. The mass forms randomly distributed air and liquid plugs under the effect of temperature difference between the cold and hot ends and the surface tension [37,38]. Due to the pressure difference between the evaporation section and the condensation section, the working fluid is driven to flow to the condensation section. The working fluid flows back to the evaporation section under the gravity action after the heat release [39]. The working process of the OHP is given in Figure 1.

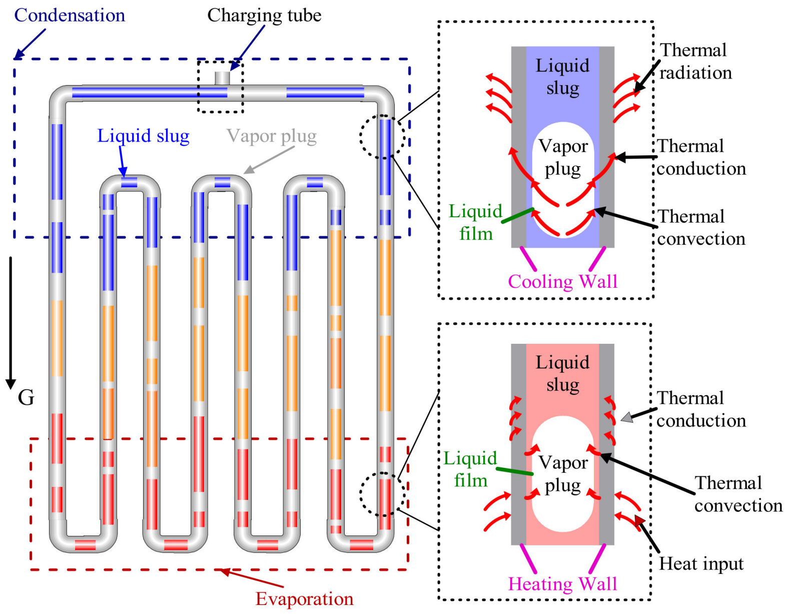

Figure 1. Working process of OHP.

There are many complex physical phenomenon and heat transfer processes in the internal operation of the OHP, including heat convection, latent heat transfer, pressure difference, temperature difference, inertial force, friction, gravity, and other factors [40], which are complex coupling processes [41,42]. When the OHP is placed vertically and the heater is located at the bottom, the thermal resistance representing the heat transfer performance of the OHP can be obtained from Equation (1) [43], after reaching a pseudo-steady state under each heating power condition.

$$R_{th} = \frac{\overline{T}_{\text{evap}} - \overline{T}_{\text{cond}}}{Q_{in}} = \frac{\frac{1}{t_a}\frac{1}{W}\int_0^{t_a}\int_0^W T_{Si}(x,L,t)dxdt - \frac{1}{t_a}\frac{1}{W}\int_0^{t_a}\int_0^W T_{Si}(x,0,t)dxdt}{Q_{in}} \tag{1}$$

where R_{th} is the thermal resistance, K/W. $\overline{T}_{\text{evap}}$ and $\overline{T}_{\text{cond}}$ are the average temperature of evaporation and condensation, respectively, K. Q_{in} is the input power, W. t_a is the time interval for time averaging, s. W and L are the width and length of the OHP, respectively, m. T_{Si} is the temperature of the silicon substrate, K. x is the horizontal coordinate, m. t is the time, s.

It is assumed that the temperature distribution of the liquid film is linearly related to the thickness of the liquid film. The total heat transferred from the heating wall to the liquid film and the heat transferred from the liquid film to the cooling wall is calculated by Equation (2) [44].

$$\begin{cases} Q_{\text{w,H}} = (T_{\text{w}} - T_{sur,\text{H}})\pi dx_{\text{H}}\lambda_l/\delta \\ Q_{w,C} = (T_{sur,\text{C}} - T_{\text{w}})\pi dx_C\lambda_l/\delta \end{cases} \tag{2}$$

where $Q_{w,H}$ and $Q_{w,C}$ are the total heats transferred from the heating wall to the liquid film and from the liquid film to the cooling wall, W. T_w is the wall temperature, $T_{sur,\text{H}}$ and $T_{sur,\text{C}}$ are the temperature of liquid film during heating and that of cooling, respectively, K. λ_l is the thermal conductivity of the liquid, W/m·K. δ is the liquid film thickness, m.

In OHPs, the liquid phase is regarded as an incompressible flow and the gas phase as an ideal gas. The temperature and pressure in each vapor plug are uniform. The temperature changes for liquid plugs and vapor plugs can be calculated by Equation (3) [45].

$$\begin{cases} c_{p,l}\rho_l A_{cr}\frac{\partial T_l}{\partial t} = h_{w,l}(T_w - T_l)S + \lambda_l A_{cr}\frac{\partial^2 T_l}{\partial l^2} \\ \frac{dT_v}{dt} = \left(Q_{v,sen} + Q_{v,lat} - P_v\frac{dV_v}{dt}\right)/c_{v,v}m_v \end{cases} \tag{3}$$

where $c_{p,l}$ is the specific heat of the liquid, J/(kg·K). ρ_l is the density of the liquid, kg/m^3. A_{cr} is the cross-sectional area of the flow path, m^2. T_w and T_l are the temperature of channel wall and liquid plug, respectively, K. $h_{w,l}$ is the heat transfer coefficient between the channel wall and the liquid plug, W/(m^2·K). S is the perimeter of the liquid plug, m. T_v is the temperature of the vapor plug, K. $Q_{v,sen}$ and $Q_{v,lat}$ are the total amount of sensible heat and latent heat, respectively, W. P_v is the pressure of vapor plug, Pa. V_v is the volume of the vapor plug, m^3. $c_{v,v}$ is the specific heat at constant volume, J/(kg·K). m_v is the mass of the vapor plug, kg.

2.2. Technical Characteristics of OHP

2.2.1. Excellent Heat Transfer Performance

Yu et al. [46] designed the 18-channel 3D-OHP with liquid metal as the working fluid, as listed in Figure 2a. The thermal resistance was as low as 0.0351 °C/W and the heat transfer performance was improved by 20.57% compared with the pure ammonia OHP. Thompson et al. [47] measured the thermal resistance data (0.08 °C/W) of a plate OHP with staggered micro-channels when the working fluid, heating mode, and heat pipe matched. Ji et al. [48] manufactured the high-temperature OHP for liquid metal. The minimum thermal resistance was 0.08 °C/W with a filling rate of 45% and a heating power of 3168 W. Ji et al. [49] tested the high-temperature vibration OHP of a liquid metal through different proportions of NaK. The minimum thermal resistance was 0.071 °C/W with 3528 W input power and a 90° inclination angle. Czajkowski et al. [50] studied the patterned OHP with a special rotation system. The thermal resistance was 0.05 °C/W when the rotation speed was higher than 200 rpm. Qu et al. [51] discovered the OHP of spherical Al_3O_3. The maximum thermal resistance of the OHP decreased by 0.14 °C/W with the filling rate of 70%. The thermal resistance of water was lower than that of ethanol [52]. Tokuda et al. [53] tested the double-loop closed OHP made of Incoloy 800 HT with sodium and the effective thermal conductivity was 2.6×10^3 to 2.3×10^4 W/(m·K). Zhao et al. [54] constructed a sizable OHP experiment to investigate the variables of thermal conductivity. The OHP had a significant thermal load with an effective thermal conductivity of 5676 W·m^{-1}·C^{-1} when the filling rate was 40%. Lin et al. [55] took aluminum materials to make interconnected rectangular channels of the OHP for heat dissipation of high-power LED, as given in Figure 2b. The thermal resistance was 0.18 °C/W with the heating power of 110 W to achieve a good heat dissipation.

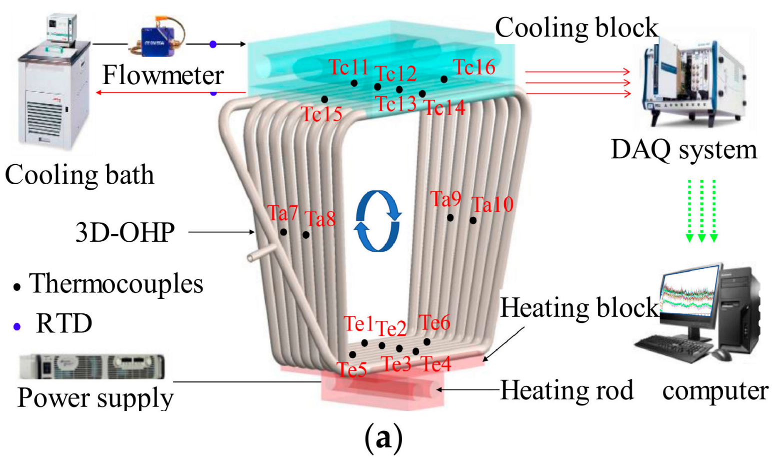

Figure 2. *Cont.*

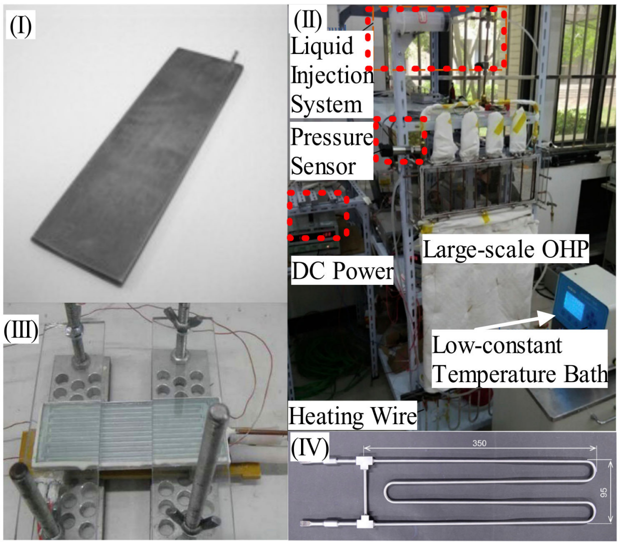

(**b**)

Figure 2. Two-dimensional and three-dimensional OHP devices. (**a**) An 18-channel 3D-OHP experimental device; (**b**) 2D OHP unit. (I) Thompson et al., (2011), [47]. (II) Zhao et al., (2017), [54]. (III) Lin et al., (2011), [55]. (IV) Tokuda et al., (2022), [53].

2.2.2. Simple Structure of the OHP with a Small Volume

The most prominent characteristics of OHPs are its miniaturization abilities and simple structure, as listed in Figure 3a. An OHP can oscillate by itself without the liquid suction core and the assistance of other equipment. Qian et al. [56] applied loop OHP to study the heat dissipation of grinding wheels. Monroe et al. [57] used a four-loop OHP to test the fluid stirring of magnets to collect energy with aluminum blocks to assist heating and cooling. Zhao et al. [58] carried out the experiment with three turns of the OHPs to achieve the thermal properties of the coupling phase change materials. Qu et al. [59] made three kinds of copper OHPs (a 2D-OHP, three-layer 3D-OHP, and four-layer 3D-OHP) and studied the coupled heat transfer of the phase change materials. Jin et al. [60] used high-temperature quartz glass to make transparent OHPs with high solar light transmittance, which can realize the experiment research of solar energy-absorbing nano-fluids. The highest thermal conductivity can be achieved when the OHP is filled with 3.0 wt.% nano-fluids. Alqahtani et al. [61] explored the influence of the bending degree of OHPs on heat transfer. There is no significant effect on the thermal performance when the bending angle increases. Iwata et al. [62] developed 10 laps of OHPs. A flexible and highly conductive tropical belt was formed, which can be used as a cooling device in a spacecraft. Wei et al. [63] clamped between commercial battery packs to simulate the thermal power generated by two adjacent battery modules, as shown in Figure 3b. The OHP was filled with the dual fluid mixed ethanol–water and the size was consistent with the length of the battery pack. The evaporation section was heated by the battery and the condensation section used fans to dissipate heat, which had a good battery cooling effect and provided a new idea for the battery cooling of electric vehicles.

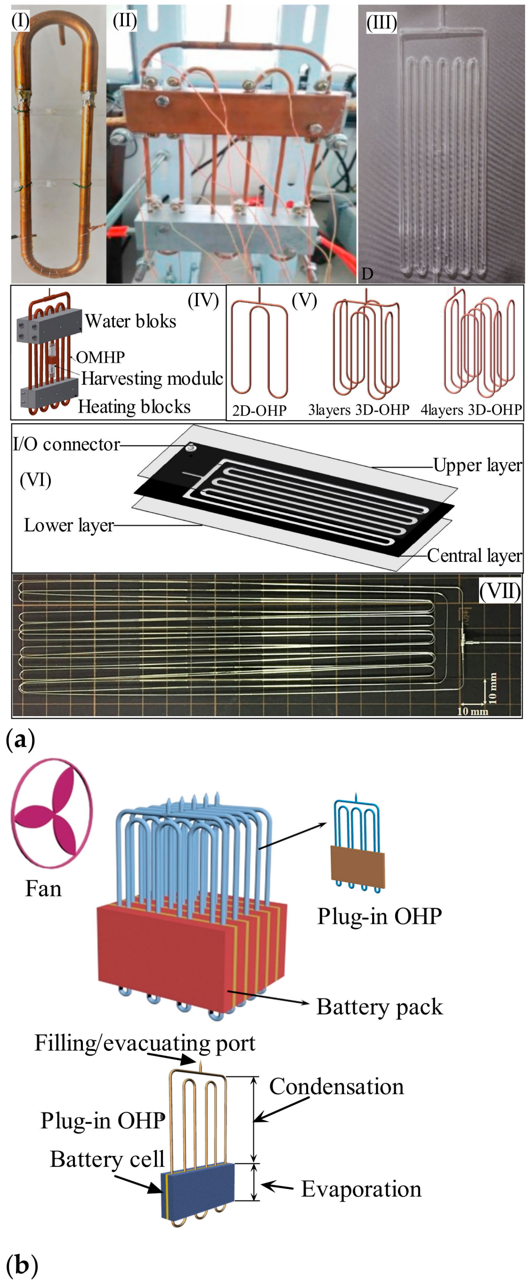

Figure 3. OHP array and distribution structure for cooling. (**a**) Multi-loop OHP array and distribution structure for spacecraft cooling; (**b**) OHP distribution for battery cooling. (I) Qian et al., (2019), [56]. (II) Zhao et al., (2016), [58]. (III). Jin et al., (2019), [60]. (IV). Monroe et al., (2018), [57]. (V). Qu et al., (2019), [59]. (VI). Alqahtani et al., (2022), [61]. (VII). Iwata et al., (2021), [62].

3. Effect of Various Filling Working Fluids of OHPs on Heat Dissipation

The common working fluids used in OHPs are nano-fluids, gases, single liquids, mixed liquids, surfactants, and SWRF.

3.1. Metal Nano-Fluid

A metal nano-fluid refers to a new type of heat transfer medium with uniform, stable, and high thermal conductivity, which is prepared by dispersing metal nano-powders into the base liquid [64]. At an appropriate concentration, nano-fluids have better thermal conductivity [65,66] and higher heat transfer limits [67] than traditional working fluids. The common nano-particles are metals (Al, Ag, Cu, Fe, etc.) and metal oxides (Al_2O_3,

Fe_3O_4, TiO_2, etc.). Table 1 demonstrates the metal nano-fluids effect on the heat transfer performance of OHPs. The heat transfer performance of the OHP can be significantly improved by the appropriate particle size [68,69], fluid concentration [70,71], filling rate [72], tilt angle [73], and heating power [74] of metal nano-particles. Furthermore, for metal nano-fluid OHPs, an applied magnetic field helps to reach the start-up faster at low heat input conditions [75,76].

Table 1. Thermal properties of metal nano-fluids.

Metal Nano-Category	Particle Size	Concentration	Liquid Filling Rate	Inclination Angle/°	Heating Power/W	Reduction of Thermal Resistance
Al_2O_3 [68]	–	0, 0.1, and 0.5 wt.%	50%	0, 90	10~80	15.8%
Al_2O_3 [69]	56 nm	0~1.2 wt.%	50%	90	20~140	25.7%
Ag [70]	50 nm	50, 200, and 600 ppm	–	–	314, 385, and 488	30%
Al_2O_3 [71]	10~30	0.5, 1, and 3 wt.%	20%, 40%, 60%, and 80%	10, 40, 70, and 90	20, 30, and 40	Improved thermal performance by 56.3%
γ-Fe_2O_3 [72]	20	2 vol.%	50%	90	0~160	12%
Fe_2O_3 [73]	20	2 vol.%	50%	0~90	10~90	24.1%
Fe_3O_4 [74]	5~20	90, 270, and 450 ppm	70%	90	20, 55, 90, 125, and 160	27.6%
Fe_3O_4 [75]	25	0.2 wt.%	50%	90	0~200	11%
$NiFe_2O_4$ [76]	25	1.5, 3 wt.%	–	90	200, 300, and 400	30.4%

Karthikeyan et al. [77] conducted an experimental study on a COHP with colloidal nano-fluids of Cu (average nano-particle size is 100 nm) and Ag (average nano-particle size is 60 nm). Compared with deionized water, the Ag nano-fluid increased the OHP heat transfer limit by 33.3% and the evaporation wall temperature was lower. The shape of the nano-particles also had an impact on the thermal resistance. Kim et al. [78] found that the OHP thermal resistance of Al_2O_3/acetone nano-fluids with spherical, brick, and cylindrical nano-particles decreased 33%, 29%, and 16%, respectively. The nano-particles effect on the thermal performance of the OHP was revealed by Jafarmadar et al. [79] with Al_2O_3, CuO, and Ag. The flow, heat transfer, and entropy generation of the OHP in the case of pure water were checked. The entropy produced by Ag was the highest. The volume concentration of nano-particles was 0.5~1%, which can minimize the generation of entropy and proper thermal operation. Goshayeshi et al. [80] studied the influence of nano-fluids on the flow and thermal properties of OHPs with Fe_2O_3/kerosene, as Figure 4 displayed. The five-flow modes were obtained of the evaporation section when the filling rate of the Fe_2O_3 nano-fluids was 50% (average nano-particle size of 20 nm with the concentration of 5 vol.%). With the increase in heat (10~80 W), the bubble flow, slug flow, foam flow, annular steak flow, and annular flow will gradually appear in the evaporation section. When the liquid plug speed was ≤ 0.15 m/s, bubbles with a diameter equal to the inner diameter of the pipe were generated. Subsequently, [81] compared Fe_3O_4/water and the effect of -Fe_2O_3/kerosene nano-fluids on the heat transfer performance. Fe_3O_4/water and -Fe_2O_3/kerosene nano-fluids reduced the thermal resistance by 30.8% and 16.7%. Gandomkar et al. [82] studied the glass and copper OHP of ferromagnetic fluid under different magnetic fields through visual experiments. The place with the magnetic field had a smaller thermal resistance and the best thermal performance of the copper OHP. The performance without a magnetic field was the best for the glass OHP. Monroe et al. [83] examined the performance of solenoid-assisted OHPs for $CoFe_2O_4$ nano-fluids. A ring magnet was used to magnetize and the $CoFe_2O_4$ nano-fluids improved the heat transfer of heat pipes by 58%.

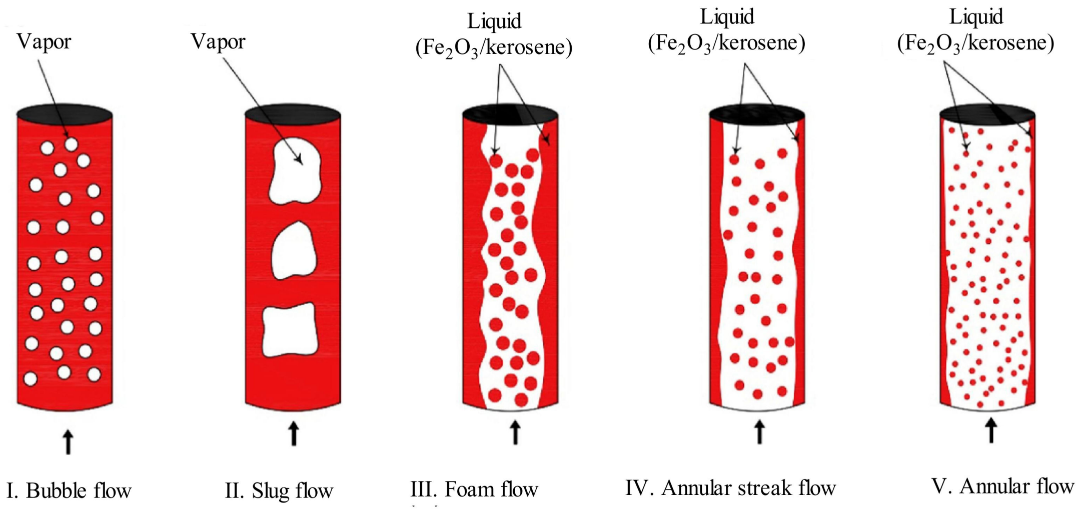

Figure 4. Flow pattern of Fe_2O_3/kerosene metal nano-fluid of OHP [80]. Goshayeshi et al., (2016).

3.2. Non-Metallic Nano-Fluid

Non-metallic nano-fluids are SiC, CNT, graphene, $CaCO_3$, and other compounds. Table 2 highlights the influence of non-metallic nano-fluids on the heat transfer performance of OHPs. In the OHP, heat transfer occurs due to repeated pressure fluctuations, with higher heat transfer occurring with more repetitions of pressure fluctuations. To provide a higher frequency of pressure and an average pressure inside the OHP, Tanshen et al. [84] used an aqueous solution of 0.2 wt.% of multi-walled carbon nano-tubes (MWCNTs) to experimentally investigate the thermal resistance and pressure fluctuations inside the OHP. Sadeghinezhad et al. [85] found through experimental studies that the deposition of graphene formed a coating on the surface of the sintered core in the evaporator section. This coating increased the surface wettability and thus improved the thermal performance of the heat pipe. Kim and Bang [86] discovered that the capillary limit of heat pipes containing graphene oxide/water nano-fluids was higher than that of the aqueous heat pipes. This is because the nano-particle coating changes the effective capillary radius and the bending moon surface, leading to an increase in the maximum fluid flow rate through the core structure. On the other hand, Wu et al. [87] showed in their study that the variation of thermal load has a greater effect on the thermal performance of the OHP than the variation of concentration. Beyond this, the addition of nano-particles to the working fluid can significantly enhance the heat transfer characteristics of the OHP and further improve the heat dissipation capacity of the OHP [88]. Zhou et al. [89] indicated that the addition of a graphene nano-sheet nano-fluid to distilled water can alleviate drying and improve the heat transfer performance of OHPs. Nazari et al. [90] reported that the addition of graphene oxide flakes improved the thermal conductivity and viscosity of the base fluid. Furthermore, the high concentration of nano-fluids reduces the thermal properties of OHPs compared to pure water, which is attributed to the increase in the dynamic viscosity of the nano-fluid. To prepare graphene nano-fluids with excellent stability, Xu et al. [91] as well as Zhou et al. [92] chose to use ethanol–water mixtures as the base fluid. In addition to this, the addition of appropriate graphene oxide nano-particles improved the OHPs initiation performance [93]. Zhang et al. [94] revealed that the addition of nano-particles promoted the phase transition of the work fluid in the OHP on the one hand, while increasing the transient velocity and driving force of the work fluid on the other hand. These are conducive to the reflux of condensate, and they can effectively avoid the dry-out phenomenon.

Table 2. Thermal properties of non-metallic nano-fluids.

Non-Metallic Nano-Fluids	Concentration	Liquid Filling Rate/%	Inclination Angle/°	Input Power/W	Reduction of Thermal Resistance
MWCNTs [84]	0.05, 0.1, 0.2, and 0.3 wt.%	60	90	50 ~400	About 36.2%
Graphene [85]	0.025, 0.05, 0.075, and 0.1 wt.%	–	0~90	20~120	48.4%
Graphene oxide (GO) [86]	0.01 and 0.03 vol.%	100	90	50 ~400	Maximum heat transfer enhancement 25%
C60 [87]	0.1, 0.2, and 0.3 wt.%	50	50	10~60	36%
Hydroxylation MWNTs [88]	0.1~1 wt.%	50	90	–	34%
Graphene Nano-sheets [89]	1.2, 2, 5.7, 9.1, 13.8, and 16.7 vol.%	45, 55, 62, 70, and 90	90	10 ~100	83.6%
Graphene oxide [90]	0.25, 0.5, 1, and 1.5 g/L	50	90	10~70	42%
Oligographene (FLG) [91]	0.1, 0.3, 0.5, 0.75, and 1 mg/mL	55	90	20~60	25.16%
Carbon nano-tubes (CNTs) [92]	0.05, 0.1, 0.2, 0.3, and 0.5 wt.%	35	90	8~56	About 66.6%
Graphene oxide [93]	0.02~0.1 wt.%	20, 50, and 80	90	10~30	54.34%
SiO_2 [94]	0.5, 1, 1.5, and 2 wt.%	50	90	10~50	40.1%

Sadeghinezhad et al. [95] studied the thermal properties of copper sintered heat pipes with graphene nano-fluids at different dip angles of 0°~70°and liquid filling rates of 30~60%. The maximum thermal conductivity of the graphene nano-fluids heat pipe (5 vol.%) was increased by 105% and the thermal resistance was reduced by 26.4%. Khajehpour et al. [96] discovered the performance of the L-shaped OHP with SiO_2 nano-fluids with different nano-particle sizes (11~14 nm and 60~70 nm). The experiment thermal resistance increased with the nano-particle size. For SiO_2 nano-fluids at 11~14 nm (0.5 wt.%), the maximum reduction of thermal resistance was about 24% at the vertical position under a heat load of 10 W and a liquid filling rate of 100%. Li et al. [97] studied the thermal performance of OHPs with aqueous ethylene glycol-based graphene nano-fluids. The minimum thermal resistance of 0.36 K/W was achieved at a thermal load of 85 W and a liquid filling rate of 35% for 2 g/L graphene nano-fluids. Choi [98] tested the thermal performance of thermosyphon heat pipes with cellulose nano-fluids, which increased the boiling heat transfer coefficient by about 71.74%.

3.3. Mixed Nano-Fluid

Both metallic and non-metallic nano-fluids are prepared by suspending a single nano-particle in a base solution to obtain a stable suspension. Mixed nano-fluids are made up of two or more different nano-particles [99]. Zufar et al. [100] studied the thermal performance of Al_2O_3-CuO/water mixed nano-fluids (0.1 wt.%) and SiO_2-CuO/water mixed nano-fluids (0.1 wt.%) under different heat inputs (10–100 W) with the liquid filling rates of 50–60%. A minimum thermal resistance of 0.27 °C/W can be obtained with SiO_2-CuO mixed nano-fluid. The thermal resistance of Al_2O_3-CuO and SiO_2-CuO mixed nano-fluids were reduced by 57% and 34%, respectively [101]. Moghadasi et al. [102] conducted a 3D numerical study on the laminar flow and heat transfer of Al_2O_3-CuO/water mixed nano-fluids in a U-shaped bend in porous media. The temperature and velocity contour of different volume fractions with water at the base fluid and mixed nano-fluids are given in Figure 5a,b, where φ is the volume fraction and r_p is the porosity. Nano-fluids are applied in the presence of porous media as fluids accumulate near the walls and enhance the heat transfer. When the volume fraction changed from 1% to 5%, the velocity distribution improved, and the temperature gradient increased. Xu et al. [103] studied the performance of thermosyphon OHPs mixed with Al_2O_3-TiO_2/water (0.2 vol.%). The conditions under different filling rates (30~70%) and coolant flow rates (0.4~0.56 L/min) were compared with 25% (Al_2O_3) and 75% (TiO_2) mixed nano-fluids, which achieved a thermal resistance reduction of 26.8% and increased the thermal efficiency by 10.6%. Mukherjee et al. [104] configured the SiO_2-ZnO/water mixed nano-fluids of different mass fractions (0.025~0.10 wt.%) and Reynolds numbers (7743~23,228). The thermal conductivity at 60 °C can be increased by up to 30% with a mass fraction of 0.10 wt.%. Veeramachaneni et al. [105] fabricated a rectangular flat loop OHP for electron cooling applications with Cu-graphene/water mixed nano-fluids (0.1~0.2 vol.%). For a mixed nano-fluid with a volume concentration of 0.02%, the capillary limit increased by 36.97% and the wall temperature of the evaporation section decreased by 9.8%. The mixed nano-fluid with a copper/graphene ratio of 30:70 can obtain a minimum thermal resistance of 0.1 K/W.

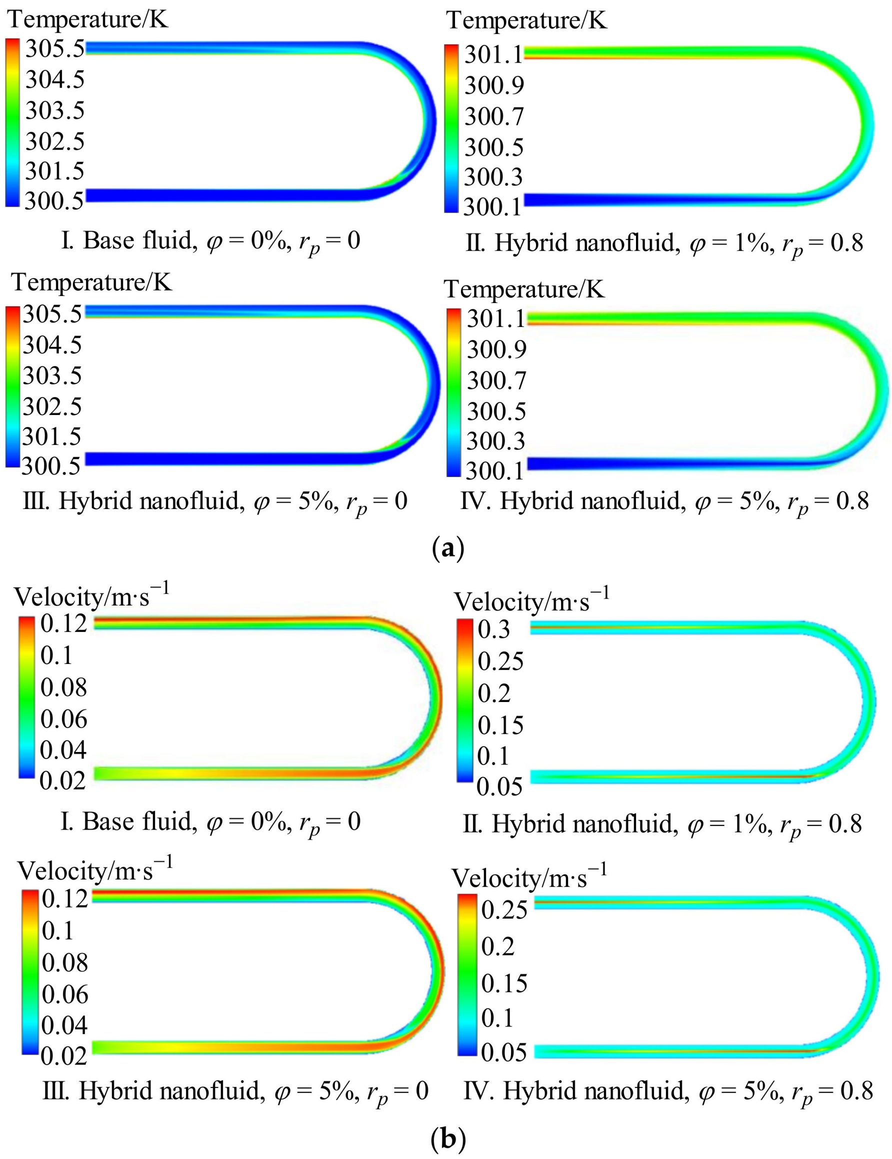

Figure 5. Temperature and velocity contours of mixed nano-fluids [102]. Moghadasi et al., (2020). (**a**) Temperature contours with mixed nano-fluids of different volume fractions. (**b**) Velocity contours using mixed nano-fluids of different volume fractions.

3.4. Gas Working Fluid

The gas can be applied as the working fluid of OHPs if the temperature of the working environment is too low. The researchers explored various gases of neon, argon, nitrogen [106,107], helium [108], and hydrogen [109,110]. Liang et al. [111,112] experimentally tested OHPs with neon, and the maximum effective thermal conductivity was 22.18 kW/(m·K) at an optimal filling rate of 24.5%. Barba et al. [113] found that the expansion and contraction of gases play an important role in the circulation of working fluids. The circulation was hindered when the filling rate was too low and the OHP could not be started normally. Sun et al. [114] simulated OHPs with hydrogen as the working fluid. The influence of hydrogen on the latent heat transfer was 45~51%, which is proportional to the volume fraction of gas. Li et al. [115] researched nitrogen as the working fluid and the thermal conductivity of the bottom heated was about 16 k W/(m·K), which was about 32 times that of pure copper. Xu et al. [116] conducted experimental studies on low-temperature OHPs filled with helium. The effective thermal conductivity was 4.8~13 kW/(m·K) with an inclination angle of 30° and a liquid filling rate of 70.8%. Fonseca et al. [117] took the experiments between 77 K and 80 K with nitrogen. The temperature difference between the OHP sections was small and the maximum thermal conductivity was 70 kW/(m·K), with a liquid filling rate of 20% [118]. The thermal performance of more than 2000 helium working fluid OHPs under the filling rate of 20~90% was tested. The liquid filling rate was 69.5% and the maximum effective thermal conductivity was 50 kW/(m·K). The non-condensable gas of the OHP reduced the evaporation amount to slow down the circulation of the working fluid, which can weaken the oscillation and reduce the heat transfer performance [119,120]. The OHP with a heat flux constant and wall temperature constant is displayed in Figure 6a. The effect of non-condensable gases on OHPs is demonstrated in Figure 6b. (Q is the heat flux, T is the temperature, and ω is the mass concentration). The higher the temperature of the evaporation section, the less influence of the non-condensable gas. Chen et al. [121] conducted a series of experiments to study the thermal performance of ethane OHPs (EOHPs) in the medium and low temperature regions (−90~0 °C). The liquid filling rate of the best performance of EOHPs was not affected by the operating temperature and heat input, which was always maintained at about 30%. The lowest corresponding thermal resistance was 0.02 °C/W at the inclination angle of 30° and the temperature of −80 °C. At a high heat input of 30~50 W, the latent heat of vaporization was the main characteristic that determined the thermal performance of the EOHP.

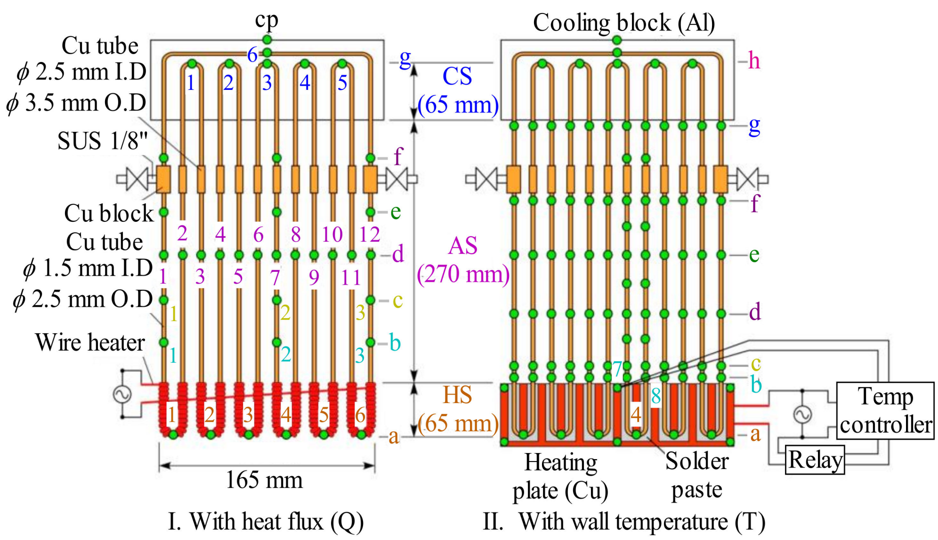

(**a**)

Figure 6. *Cont.*

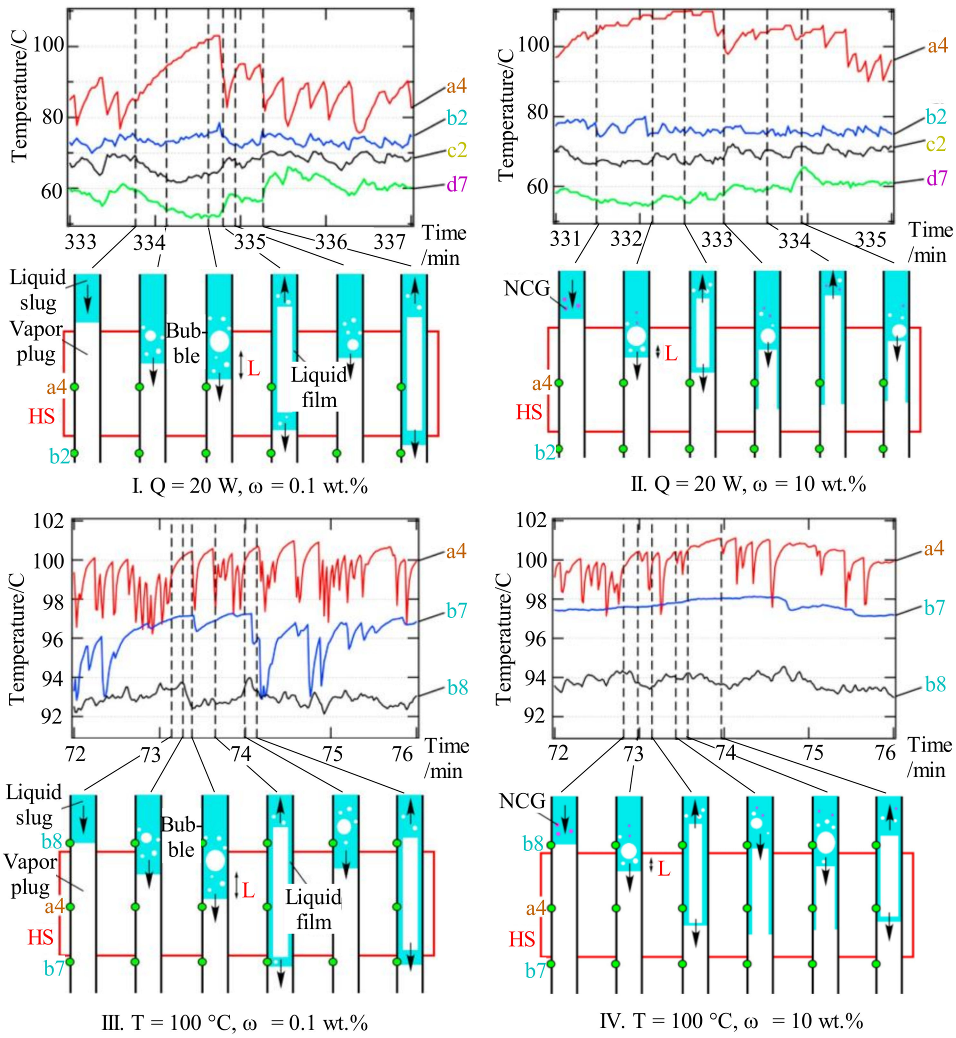

(**b**)

Figure 6. Effect of non-condensable gas on heat pipe [120]. Senjaya et al., (2014). (**a**) EOHP with heat flux constant and wall temperature constant. (**b**) Measurement point temperature status and flow image of OHP.

3.5. Organic Solvent

Table 3 summarizes some trends in the heat transfer performance of OHPs with different organic solvent liquids as the working fluids. From the information in Table 3, the working fluids, filling rate, input power, lowest thermal resistance, and lowest thermal resistance obtained from the nine papers are compared. At a low heat input, the heat transfer depends strongly on whether the oscillations are triggered or whether the oscillatory flow is triggered fast. In contrast, the effect of viscosity on the heat input and the effect of the latent heat of vaporization increases at a high heat input. It can be concluded from Table 3 that the choice of the working medium and filling ratio should be determined according to the actual situation. In terms of taking full advantage of low thermal resistance, 50% is a good filling ratio for ethanol, which should have a low heat input. In the case of a large filling ratio and large heat input, methanol is a better choice. Acetone has a good fill ratio of 50–70% with high heat input. The best filling ratio for Ionic liquids is about 44% with high heat input. The LiCl solution performs well at a 62% filling rate. R1233zd (E) with a filling rate of about 50% at moderate heat input is also an option.

Table 3. Heat transfer performance with different organic solvent liquids as working fluids.

Working Fluids	Filling Rate/%	Input Power/W	Lowest Thermal Resistance/°C·W^{-1}	Lowest Thermal Resistance Obtained
Ethanol [122]	0, 25, 37.5, 50, 62.5, 75, and 100	–	0.95	50%
Methanol [123]	20~95	5~100	0.2	95% and 100 W
Ethanol [124]	50	15~50	0.6244	50 W
Acetone [125]	50 ± 5% and 70 ± 5%	60~300	0.092	70% and 260 W
Lonic liquids [126]	65 ± 5	50~250	0.15	44.4% and 250 W
Acetone [127]	50	10~200	0.14	200 W
LiCl solution [128]	45, 55, 62, 70, 80, and 90	10~100	0.9	62% and 10 wt.%
Acetone [129]	0~100	10~120	0.39	60% and 100 W
R1233zd(E) [130]	40~70	0~200	0.1184	50% and 70 W

Takawale et al. [131] studied the performance of FPOHPs and capillary tube OHPs (CTOHPs) under different heat inputs (20 W~180 W) and liquid filling rates (40%, 60%, and 80%). After ethanol was filled into the OHP, the thermal resistance of the FPOHP and CTOHP decreased by 83% and 35%, respectively. Bastakoti et al. [132] tested the heat transfer performance of OHPs with methanol, ethanol, cetyltrimethylammonium chloride (CTAC), and deionized water as the working fluids. The heat pipe charged into the CTAC had the lowest thermal resistance of 0.30 K/W. The thermal resistance of the OHP with deionized water, methanol, ethanol, and acetone as the working fluid tended to increase after the heating power reached 65 W identically [133]. Bae et al. [134] established a numerical model of the OHP and simulated the change in the liquid film thickness. The numerical model was based on a 1D piston flow hypothesis. Figure 7a is a schematic diagram of two vertical heat pipes. Figure 7b is the plug flow on the *z*-axis. Figure 7c is a piston flow. Figure 7d is the liquid plug. Figure 7e is the plug (bubble). Figure 7f is the liquid film. Figure 7g is the pipe wall. The simulation results had an error of less than 20% compared with the experimental data, which proved that the oscillation prediction of fluids needs to consider membrane dynamics.

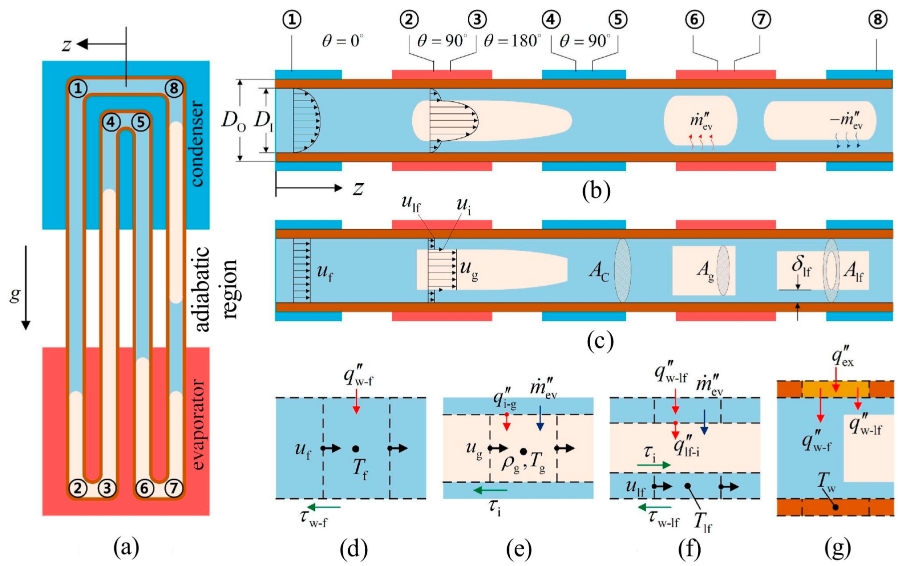

Figure 7. Schematics of vertical heat pipe and control volume analysis [134]. Bae et al., (2017). (**a**) Schematic. (**b**) Plug flow on z-axis. (**c**) One-dimensional plug flow. (**d**) Liquid slug. (**e**) Vapor plug. (**f**) Liquid film. (**g**) Wall.

Sun et al. [135] studied the hydro-thermodynamic behavior of the ethanol-based bubble distribution, bubble motion, and temperature of the working fluid. The proportion of small-sized bubbles increased with the improvement in the liquid filling rate and heating power. The proportion of medium-sized and large-sized bubbles decreased when the oscillation frequency and amplitude of bubbles increased. The high boiling point fluid working fluid heat pipes was studied by Mahapatra et al. [136] using the Buckingham's pi theorem to perform a dimensionless analysis of the heat transfer performance. High boiling point working fluids alleviated locally high heat flux densities. Xue et al. [137] conducted a novel full-visualization experiment on ammonia water OHPs with a high-speed camera. As the heating power increased, the flow pattern changed from a stopper flow to a ring flow and the proportion of evaporation heat increased from 7.7% to 32.4%. Liu et al. [138] analyzed the starting performance of the OHP based on system identification theory. The working fluids with small dynamic viscosity, small specific heat, and large saturation pressure gradients favored the start-up of OHPs. Hao et al. [139] studied the effect of polytetrafluoroethylene with ionized water, ethanol, and acetone as the working fluids on the heat transfer performance. When acetone was used as the working fluid, the liquid plug oscillation amplitude and speed were the highest and the thermal resistance was 30~63% lower than that with water as the working fluid.

3.6. Mix Liquids

Different pure working fluids have their own advantages under working conditions. Non-azeotropic mixtures have the characteristics of phase change and temperature fluctuation, which can make the heat source and working fluid well-matched [140]. The mixture plays the superior characteristics of each different components, which cause the OHP to achieve better start-up and heat transfer performances [141]. Zhu et al. [142] concluded that the thermal resistance of the OHP was filled with a ketone-pure–water mixture. When the filling rate was high, the thermal resistance of the OHP filled with pure water and acetone was 45.8% and 38.7% lower than that of the ketone-pure–water mixture. The mixture had better resistance to dryness at a low liquid filling rate [143]. Shi et al. [144] studied the OHP with ethanol–water, ethanol–methanol, and ethanol–acetone as working fluids with different mixing ratios. When the filling rate was increased to 62%, the heat transfer performance of OHPs with pure working fluids was better than that with mixed working fluids. When the filling rate reached 70%, the thermal resistance of the different working fluids tended to be approximated with the increase in the heating power. When the filling rate was low, the methanol working fluid can inhibit the drying up of the OHP [145]. Xu et al. [146] tested the effect of HFE-7100 and the lowest thermal resistance was 0.1634 °C/W with the mixing ratio of the working fluid was 1:2. Chang et al. [147] obtained the internal pressure of methanol-deionized water OHPs with different mass ratios. When the mass ratio of binary working fluid methanol and deionized water was 1:5, the starting performance of the OHP was the best with the temperature of 80 °C, the thermal resistance of 0.114 °C/W, and the heat flux density of 1.47 W/cm^2.

Markal and Varol [148] studied the effects of the volume mixing ratio, inclination angle, and fill ratio on the OHP thermal performance of ethanol (E)–pentane (P) mixtures under different heat inputs. The ethanol–pentane mixture exhibited lower thermal resistance and had the best thermal performance with the filling rate FR of 30%, the dip angle IA of 90°, and the mixing ratio E:P of 1:3. Under the same filling rate and inclination conditions, the ternary mixture of deionized water (W), methanol (M), and pentane (P) had a better thermal performance when the mixing ratio was 1:2:3, as shown in Figure 8. The best thermal performance occurred when the filling rate was 50% [149]. Compared with the two binary mixtures of ethanol–pentane and methanol–pentane, the overall performance of the ternary mixture was low. Markal and Varol [150] also compared the effects of pentane–methanol, methanol–hexane, and water–methanol–pentane mixtures on OHP thermal properties. The immiscible pentane–methanol (P:M = 1:1) mixture had better thermal properties than the mixture of hexane–pentane.

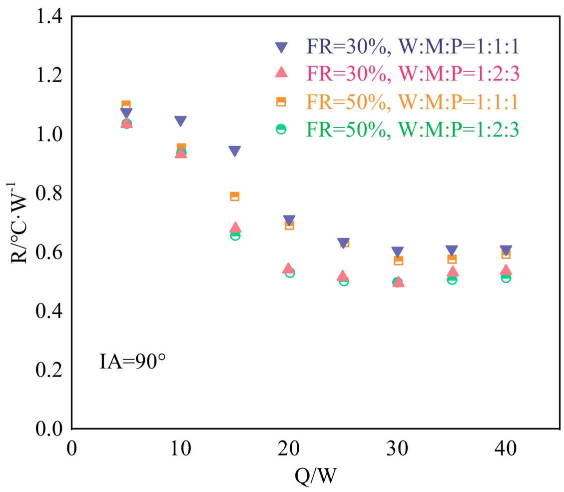

Figure 8. Change in thermal resistance with heat load for each mixture under different mixing ratios [149]. Markal et al., (2021).

3.7. Surfactants and Self-Rewetting Fluids

When the working fluid flows in the MCOHP, the flow of the working fluid will be affected by resistance due to the presence of surface tension. The surface tension of the working fluid can be reduced if surfactants are added. The capillary resistance can be reduced and the heat transfer performance of the OHP can be improved [151,152]. Hao et al. [153] conducted a series of experiments to study the effects of super-hydrophilic and hydrophilic surfaces on the segment plug motion of OHPs. The influence of surface wetting characteristics on the gas–liquid interface at the end of the plug is shown in Figure 9. The length of the film in super-hydrophilic OHPs is significantly increased. Compared with the copper OHP, the thermal resistance of the super-hydrophilic and hydrophilic OHP were reduced by about 5~15% and 15~25%, respectively. Xing et al. [154] obtained OHPs with a cetyltrimethylammonium bromide (CTAB) solution as the working fluid, which can reduce the surface tension of the solution and the contact angle. The thermal resistance of 0.25 wt.% of the CTAB solution is reduced by 48.5% with the filling rate of 50%. The addition of surfactants can increase the critical heat flux density of the heat pipe by 1.26 times with the enhancement of pressure fluctuations [155]. Compared with deionized hydraulic working fluid heat pipes, the thermal resistance of the cetyltrimethylammonium chloride working fluid was reduced by 4.78% [156], which prevents drying up. Bao et al. [157] experimentally proved that the thermal resistance of OHPs that had surfactants as the working fluid was reduced by a maximum of 27.8%.

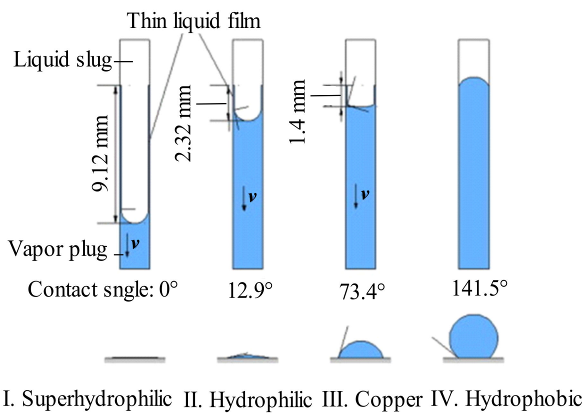

Figure 9. Schematic of the liquid–gas interface in super-hydrophilic, hydrophilic, copper, and hydrophobic OHPs [153]. Hao et al., (2014).

Abe et al. [158] proposed the concept of SRWFs by the physical properties of dilute aqueous solutions with high carbon alcohols. A SRWF enhances the heat transfer performance and heat transfer limit of OHPs with an incensement of the surface tension and a reduction of the contact angle [159]. Hu et al. [160] used a heptanol–aqueous solution to study the enhancement effect of SRWFs. The characteristics of SRWFs caused the working fluid to be spontaneously wetted in the overheated part of the tube. Wu et al. [161] applied butanol at a concentration of 6% as a working fluid for performance testing. The critical heat load was 650 W, and the total thermal resistance was 0.25 °C/W with a reduction of 60%. The SRWF nano-fluids exhibited an excellent heat transfer performance over the entire heat load range, with a maximum enhancement rate of approximately 15% [162]. The influence of a SRWF nano-fluid base prepared by mixing graphene oxide dispersion with an n-butanol–aqueous solution on OHPs had been studied [163]. The following percentages, 0.07 wt.% and 0.7 wt.% were the optimal concentrations of graphene oxide and n-butanol. The heat transfer performances were increased by 16% and 12% compared with the SRWF and nano-fluid. Savino et al. [164] performed a microgravity heat pipe experiment. They researched working fluids including aqueous alcohol solutions, multi-component brine and nanoparticle suspensions. It was shown that self-rewetting brines and self-rewetting nanofluid brines have good thermal properties. Wang et al. [165] conducted numerical studies on CLOHP with different wettability (contact angles of 5°, 33°, 147°, and 175°). Figure 10 shows the volume fraction of the liquid and vapor distribution at a heat load 20 W. Compared with superhydrophobic surfaces, CLOHPs on super-hydrophilic surfaces had a 10.8% reduction in thermal resistance at an input heat load of 20 W.

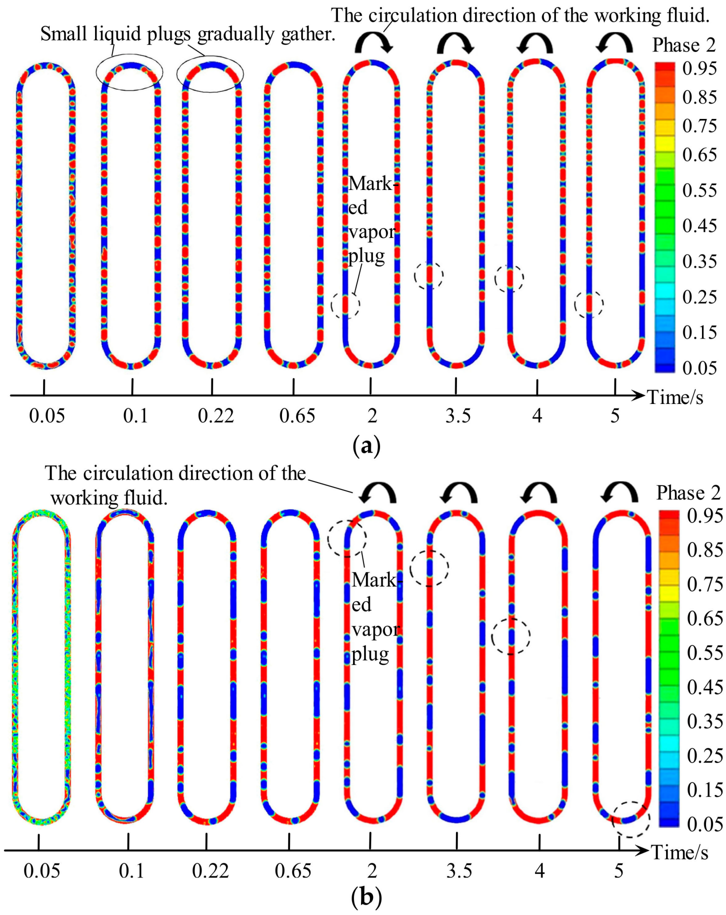

Figure 10. Volume fraction of liquid and vapor at heat load 20 W [165]. Wang et al., (2020). (**a**) Volume fraction of liquid and vapor at heat load 20 W and contact angle 147°. (**b**) Volume fraction of liquid and vapor at heat load 20 W and contact angle 33°.

4. Effect of In-Tube Flow State on Heat Dissipation Properties

The heating method, effect of gravity, characteristics of the flow pattern, and the oscillatory characteristics have influences on the heat dissipation properties.

4.1. Different Heating Method of Evaporation Section

An OHP has a very flexible use, which is reflected in its ability to heat in different positions; for example, its heating methods can be pulse heating, alternating heating, and continuous heating, and it can have a number of evaporation and condensation sections. Lin et al. [166] used vertical bottom heating to study the heat transfer performance of OHPs. The pulse heating method had a lower temperature difference than the continuous heating method [167]. Zhao et al. [168] found that the advantages of thermal resistance were pulse heating, alternating heating, and continuous heating. Taft et al. [169] compared the heat transfer performance of OHPs under DC and pulse modulation input modes. Chu et al. [170] used asymmetric heating to study a 3D helix OHP. The non-uniform heating method of multiple heat sources has also been studied in series with a two-channel flat OHP [171], as given in Figure 11a.

Mangini et al. [172] studied the heat transfer performance of hybrid OHPs in the super/microgravity environment and the non-uniform heating configuration promoted the net circulation of the fluid in the preferential direction, which improved the thermal performance relative to uniform heating. Peng et al. [173] took the bottom heating method to perform a numerical simulation study on the completely non-linear thermo-mechanical finite element model OHP. Qu et al. [174] used vertical and horizontal heating methods to study 3D-OHP. Yasuda et al. [175] studied flat-plate OHPs made of aluminum alloy by bottom heating and top heating. Lim et al. [176] used local heating to study the flat MOHP. As listed in Figure 11b, the heating method will directly affect the internal flow.

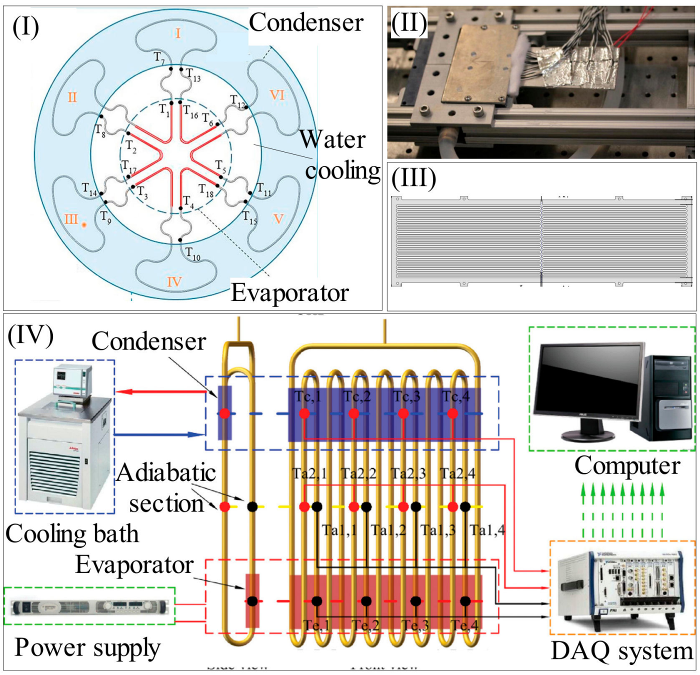

(a)

Figure 11. *Cont.*

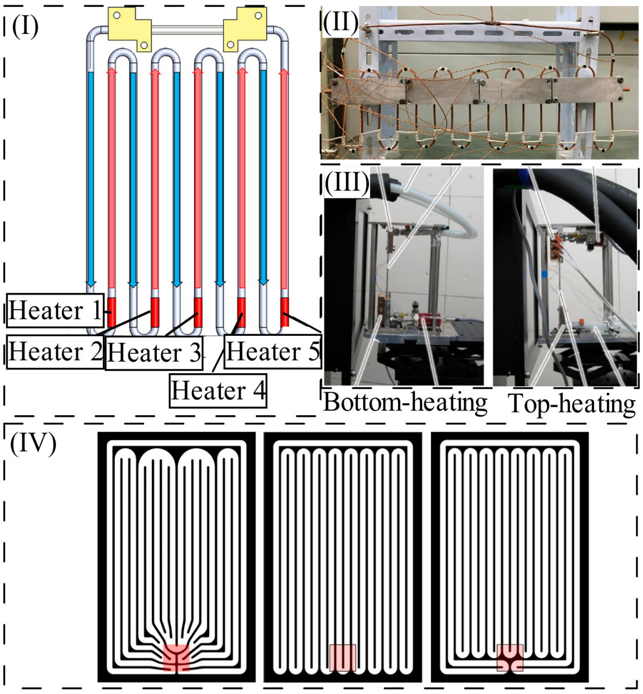

(**b**)

Figure 11. OHP for different heating methods. (**a**) OHP pulse heating and asymmetric heating method; (**b**) OHP for non-uniform heating and local heating. (I) [168]. Zhao et al., (2019); (II) [169]. Taft et al., (2017); (III) [171]. Chen et al., (2021); (IV) [170]. Chu et al., (2022); (**b**) OHP for non-uniform heating and local heating: (I) [172]. Mangini et al., (2017); (II) [174]. Qu et al., (2017); (III) [175]. Yasuda et al., (2022). (IV) [176]. Lim et al., (2021).

4.2. Flow State

E et al. [177] established a CLOHP model using the VOF (volume of fluid) method as the solution scheme to numerically simulate the liquid vapor in the two-phase conversion process. The distribution and fluctuation relationship of the pressure and vapor flow mode during the start-up under different vacuum degrees was determined. The interphase mass transfer due to evaporation and condensation in the VOF method can be applied to energy jump conditions, the Tanasawa model, and the Lee model [178]; the relevant equations are given in Table 4.

Table 4. Numerical model of interphase mass transfer.

Content	Remarks
Energy jump conditions [179] $$\dot{m} = -\frac{\left(L_v + (c_{p,l} - c_{p,v})(T_{sat} - T_{\text{int}})\right)}{[-k_{lv}\nabla T \cdot \vec{N}]_\Gamma} \quad (4)$$	$\dot{m}$ is the phase change local mass flow rate, kg/(m^3·s). L_v is latent heat. $c_{p,v}$ is constant pressure specific heat of vapor, J/(kg·K). T_{sat} is the saturation temperature associated with the considered pressure, K. T_{int} is the local interface temperature, K. k_{lv} is thermal conductivity, W/(m·K). $\vec{N}$ is the normal vector pointing in the direction of the gas phase at the Γ of the interface.
Tanasawa model [180] $$\dot{m} = \frac{2\gamma}{2-\gamma}\left(\frac{M}{2\pi R_g}\right)^{1/2}\frac{\rho_v L_v (T_{if} - T_v)}{T_v^{3/2}} \quad (5)$$	γ is the adjustment factor. M is the molecular weight. R_g is a general gas constant. is 8.314 J/(mol K). ρ_v is the density of vapor, kg/m^3. T_{if} is the interface temperature, K.
Lee model [181] $$\begin{cases} \dot{m}_{lv} = \alpha_l \rho_l \frac{c_{p,l} T_{sat}}{L_v} \cdot \frac{T_l - T_{sat}}{T_{sat}}, T_l > T_{sat} \\ \dot{m}_{vl} = \alpha_v \rho_v \frac{c_{p,v} T_{sat}}{L_v} \cdot \frac{T_{sat} - T_v}{T_{sat}}, T_{sat} > T_v \end{cases} \quad (6)$$	$\dot{m}_{lv}$ is the mass transfer of each time step in the evaporation process, kg/(m^3·s). $\dot{m}_{vl}$ is the mass transfer of each time step in the condensation process, kg/(m^3·s). α_l and α_v are the volume fraction of liquids and vapors.

The heat exchange units established by Nuntaphan et al. [182] can be used to evaluate the efficiency of the heat exchanger and the heat transfer coefficient of the air side. Qian et al. [183] proposed a novel heat transfer prediction model based on an extreme gradient boost algorithm and studied the design and cooling method of OHP prototypes during optimized processing. Sun et al. [184] established a model to study the oscillatory motion characteristics of liquid plug and vapor plug/bubble in OHPs. Nemati et al. [185] used numerical models to study the heat transfer mechanism of OHPs and predict heat transfer capacity, which simulated the oscillation behavior of the liquid plug, considering the thickness of the liquid film in the evaporation and the decrease in the liquid film thickness caused by evaporation. Daimaru et al. [186] proposed a numerical simulation method for OHPs with a check valve and new modeling features, including the pipe wall energy equation. The check valve model included pressure loss, the detailed boiling algorithm, and the pressure loss of a bending surface transformation. The temperature error of the heating section was less than 1.7 °C. Adachi et al. [187] developed transient models of fluid conditions to reproduce transmission lines. Odagiri et al. [188] combined thermo-fluid behavior in channels with thermal diffusion in OHP casing segments, which was in good agreement with the multi-branch OHP experiment results with a channel diameter of 1 mm and several turns of 42 turns.

4.3. Gravity Effect

Gravity has an important effect on the flow and circulation of the working fluid of OHPs. The gravity prevents the working fluid from flowing to the evaporation section in the top heating mode. The gravity promotes the flow of the working fluid to the evaporation section in the bottom heating mode. For micro-gravity research, the European Space Agency used parabolic flights of aircrafts to create different gravity environments. The variation of the tilt angle changed the flow pattern inside the OHP, resulting in different performance levels [189]. Mameli et al. [190] studied the OHP under different gravities. The change in gravity had a greater effect on the heat transfer performance of the OHP in the case of vertical heating compared with horizontal heating. The FC-72 working fluid was investigating the effect of gravity on the heat transfer performance at different heating powers [191]. The thermal resistance of vertical heating was lower than that of horizontal heating under the influence of gravity. The vertical heating was not as stable as the horizontal heating during operation. Ayel et al. [192] reported that closed-loop FPOHPs can respond to gravity changes more quickly and reach a steady state. Mangini et al. [193] tested the sudden loss of buoyancy and activated the oscillating segment plug/stuff flow state in micro-gravity, which had the lowest starting power. Cecere et al. [194] discovered that FPOHPs with SRWF (butanol–water) were easier to keep working under micro-gravity and a low heating power. Xing et al. [195] examined the effect of gravity on OHPs with a surfactant solution as the working fluid. The influence of gravity on the OHPs of the CTAB solution was relatively small. When the heating power was higher, the heat transfer performance of the CTAB solution OHP was stronger and the thermal resistance was reduced by 51%. Pagliarini et al. [196] trained the OHP used for the International Space Station in microgravity, where the two states of the working condition included intermittent flow (episodic fluid motion occurring in some channels) and full activation (steady fluid movement throughout the adiabatic section). The fully activated state is given in Figure 12. No significant variation between channel behaviors is observed with stable oscillations, high heat flux amplitude, and oscillation frequency. The heat flux amplitude increased almost linearly, 1500 W/m^2 at 202 W, with the power input from 1100 W to 202 W.

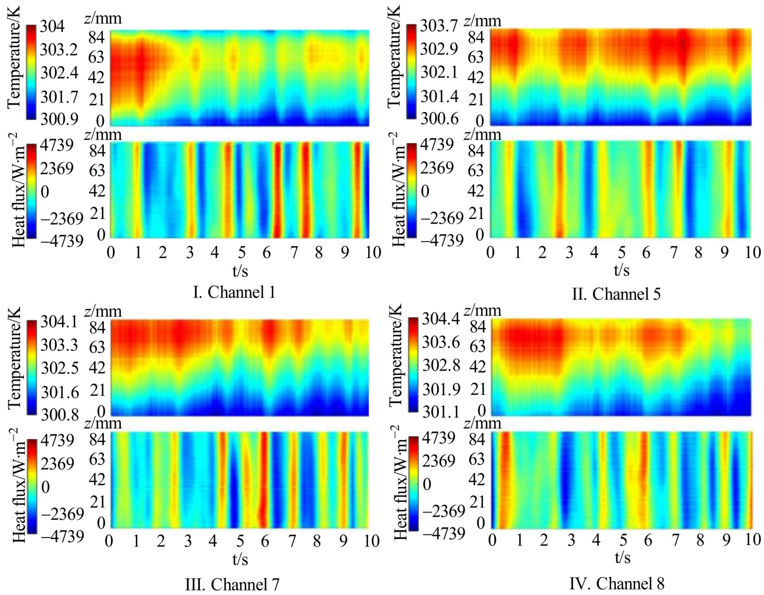

Figure 12. Wall temperature and heat fluxes in different channels under 202 W power input with stable microgravity conditions [196]. Pagliarini et al., (2021).

4.4. Characteristics of Flow Pattern in Tube

Awareness of flow boiling and two-phase instability are important parts of understanding the complex phenomena and developing OHP technology, to explore the physical mechanisms controlling the complex unsteady flow boiling heat transfer and two-phase phenomena [197], which provide insight into the heat and mass transfer relationships in OHPs. With the change in the OHP working stage, the flow pattern of the working fluid in OHPs also changes, which can directly affect the flow mode of the working fluid and the heat and mass transfer efficiency of OHPs. Yuan et al. [198] established a flow model of the liquid plug based on the Lagrange method. Liquid plug oscillation amplitude and angular frequency depend on the geometry of the OHP and the liquid filling rate. When the flow type is slug flow, the sensible heat transfer can account for more than 80% of the total heat transfer. Karthikeyan et al. [199] employed high-resolution infrared thermography to measure the flow characteristics inside OHPs. The flow is the working fluid without internal oscillation, intermittent oscillation, or continuous local oscillation. With the increase in heating power, the thermal resistance decreased from 1.90 K/W to 0.24 K/W. Spinato et al. [200] used time-strip image processing techniques to study the two-phase flow of the OHP. Low amplitude/high amplitude oscillations, cyclic oscillations, backflow, and steady cycles were observed. The nucleation and rapid growth of bubbles in the U-bend of the evaporation section lead to the transition of the working fluid from the circulating to the oscillating state. Xian et al. [201] visualized the flow behavior in an OHP duct with pulsed heating. The liquid film was thinner in pulsed heating than in continuous heating. Under the condition of a short period of pulse heating, the proportion of bubble flows increased. The flow pattern is the same as for continuous heating. Pouryoussefi et al. [202] worked with numerical methods to simulate the chaotic behavior of fluids, as listed in Figure 13. Volume fraction contours are provided for different time points for two different operating conditions (red is vapor and blue is liquid). Figure 13a is the volume fraction diagram of the OHP under a time series of 0.8 s, 2.5 s, 3.8 s, 5.5 s, 13 s, and 18 s, with the evaporation temperature T_h = 145 °C, the condensation temperature T_c = 35 °C, and the liquid filling rate of 30%. Figure 13 b presents the volume fraction plots for the time sequences of 2.2 s, 3.8 s, 5.8 s, 10 s, 16.5 s, and 18.6 s, with T_h = 150 °C, T_c = 35 °C, and a 60% filling rate. The relevant dimension increases by promoting the filling rate and evaporation temperature.

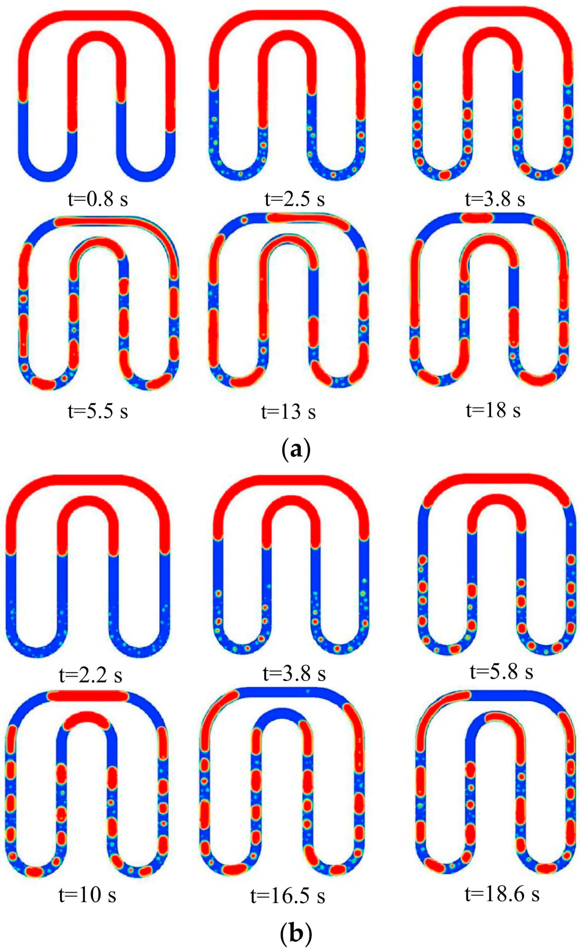

Figure 13. Volume fraction contours after formation of fluid flow [202]. Pouryoussefi et al., (2016). (**a**) Th = 145 °C, Tc = 35 °C, and 30% liquid filling rate; (**b**) Th = 150 °C, Tc = 35 °C and 60% liquid filling rate.

Feldmann et al. [203] simulated turbulence in a pipe at different Womersley numbers and found that disturbance energy is required to trigger the non-linear transition process in the subcritical state. Pouryoussefi et al. [204] modified the chaotic flow in a heat pipe based on the VOF method. There was an upper limit to the accuracy of the simulation as the fluid filling rate and heating power increased. The optimal filling rate and minimum thermal resistance were measured to be 60% and 1.62 °C/W. Mangini et al. [205] demonstrated the reliability of the infrared visualization of two-phase flows with a maximum error of ±1.5 °C in combination with a high-speed camera capable of detecting the wetting and drying of liquid films. Xia et al. [206] studied the properties of unsteady flows in parallel micro-channels. Continuous two-phase unsteady boiling often occurred when the flow rate and heat flow density were greater than 607.6 kg/m^2 and 30 W/cm^2. This phenomenon can be suppressed by increasing the forced convection heat transfer of 100% or increasing the flow boiling heat transfer of 50%. Yoon et al. [207] investigated the oscillation frequency of the liquid plug with a MOHP. The heat input can change the vapor temperature and affect the oscillation frequency. The oscillation frequency increased with the increase in the heat input. The liquid plug with a longer total length of the heat pipe had a lower oscillation frequency. Ling et al. [208] found that the heat pipe temperature fluctuated greatly during the stable circulation of the working fluid. Noh et al. [209] used a numerical model to simulate the heat transfer between the tube wall and the liquid slug/vapor plug and proposed guidelines for designing heat pipes. Figure 14a is the liquid slug and vapor plug distributions for a two-turn heat pipe with an input power of 50 W (t = 145 s) and a twenty-turn OHP with an input power of 48 W (t = 80 s). Figure 14b illustrates the heat flux distribution for the two heat pipes and Figure 14c presents the wall temperature distribution for the two OHPs. After the pseudo-steady state, the liquid slug in the two-loop heat pipe oscillates and shows a net circulating flow.

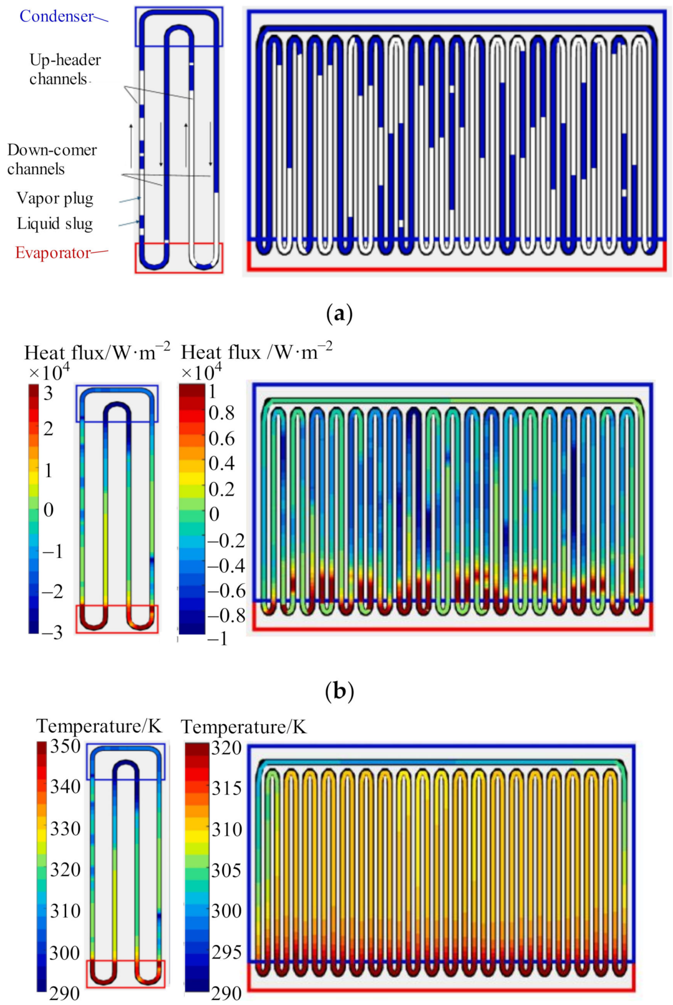

Figure 14. Heat pipe visualization data graph [209]. Noh et al., (2020). (**a**) Distribution of liquid slug and vapor plug. (**b**) Heat flux distribution. (**c**) Wall temperature distribution.

Ahmad et al. [210] investigated the heat transfer performance as a function of the flow pattern using OHPs with ethanol. The thermal resistance at a 50% filling rate was as low as 1.6 °C/W. Vo et al. [211] performed visualization experiments on the OHP and found that the cyclic motion dominated the motion of the working fluid. A 3D computational fluid dynamics model of the OHP was developed and the k-ε turbulence model was applicable to the heat pipe simulation. Schwarz et al. [212] discovered through visualization experiments that the thermal resistance of the fluid inside the heat pipe during start-up is constant at 0.43 °C/W when there is no flow (25 W to 75 W). The thermal resistance dropped to 0.34 °C/W (200 W)~0.36 °C/W (100 W) at an average velocity of 240 mm/s.

4.5. Oscillatory Characteristics

The pulsed heat pipe is a kind of non-equilibrium, passive two-phase heat transfer device with complicated internal transmission process. The heat transfer performance of OHPs depends on the oscillation degree and stability of the self-sustained oscillating two-phase flow, which leads to its unique heat transfer characteristics [213]. Yoon et al. [214] observed that the internal oscillation frequency of the OHP was between 40 Hz and 50 Hz.

Spinato et al. [215] examined the flow behavior inside the OHP using time-slot image processing technology. The flow pattern changed from oscillating to circulating state while the main frequency changed from 1.2 Hz to 0.6 Hz. Dilawar et al. [216] researched the oscillating two-phase flow in a micro-channel based on a numerical model. The pressure loss of the oscillating two-phase flow at the bend of the tube reduced the oscillation amplitude and weakened the heat transfer performance. Kato et al. [217] investigated the OHP consisting of a single straight pipe and open pipe. The heat transfer performance was enhanced with an increased amplitude of the oscillatory flow. Liquid exchange due to the oscillatory motion significantly enhanced the heat transfer with an effective thermal conductivity of up to 40 kW/(m·K). Miura et al. [218] studied liquid column oscillations with a forced oscillator. The evaporation of liquid film produced by the oscillation of working fluid is the main process of latent heat transfer. Both evaporation and condensation occur on the liquid film on the wall of micro-channel. Daimaru et al. [219] processed oscillation data based on a fast Fourier transform and mutual analysis. The vapor plug received or applied energy according to the direction of propagation. Das et al. [220] suggested a theoretical model considering the two-phase oscillatory equilibrium, which was calculated in good agreement with the experiment results. Jung et al. [221] evaluated the effect of the oscillation amplitude of a miniature OHP on the heat transfer performance. When the input power was 16 W, the time-resolved distribution of the heat flux and the corresponding flow visualization after the miniature OHP reached the pseudo-steady state are given in Figure 15. The total heat transfer rates of the evaporation and condensation sections were 14.4 W and 14.2 W, while the average value of latent heat ratio increased from 54.8% to 81.9%. When the input power increased from 7 W to 16 W, the oscillation amplitude increased from 3.4 mm to 8.3 mm, with a 13.5% reduction in thermal resistance. The oscillating motion of the liquid slug and vapor plug in the OHP promoted the heat transfer between the evaporation section and the condensing section. The oscillation amplitude and frequency are important parameters for estimating the heat flow density in OHPs [222].

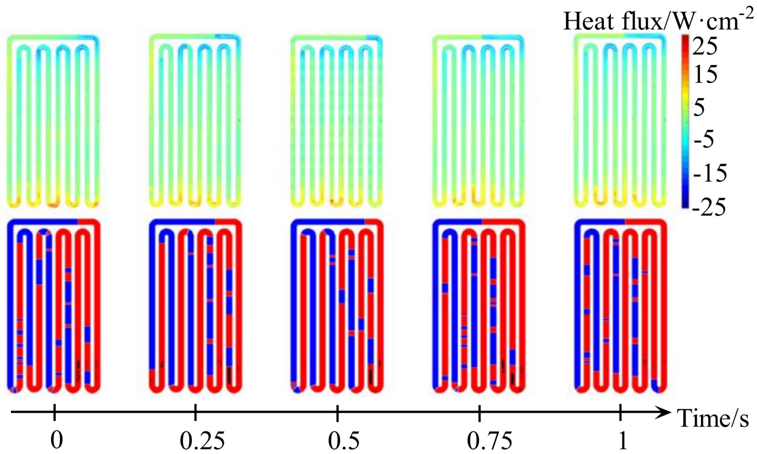

Figure 15. Time-resolved distribution and flow visualization of heat flux with input power of 16 W [221]. Jung et al., (2021).

Pai et al. [223] introduced a non-linear thermal model based on a U-shaped three-plug OHP. When the ratio of liquid slug mass or vapor plug length to the tube cross-sectional area decreased, the initial air pressure, liquid filling rate, gravity, and the oscillation frequency increased. As the temperature difference or heat transfer coefficient between the evaporation and condensation sections increased, the liquid filling rate or the initial temperature decreased. Perna et al. [224] tested the main frequency of pressure signal oscillation in the evaporation and condensation sections under micro-gravity. The main frequency of the pressure signal was in the range of 0.6~0.9 Hz, which increased with the heating power. Simplifying the entire OHP into a single unit can facilitate the study of various parameters of oscillation behavior [225]. Rao et al. [226,227] investigated self-sustained thermally driven oscillating in micro-channels. The motion of the meniscus generated a liquid film on the tube wall. The thickness of the liquid film and length at a given time determined the overall dynamics of the meniscus. Fourgeaud et al. [228] examined the variation of the liquid film thickness on the tube wall based on a single branch OHP. The film thickness was larger compared with the wedge-shaped film in a capillary OHP.

5. Bibliometric Study and Analysis

The OHP was first proposed in the 1990s and it has aroused wide attention in the academic circle. Scholars around the world have published a lot of research in this field. In order to understand the data from the relevant literature, we analyzed the literature on the oscillating heat pipe from the Web of Science Core Collection (WOSCC) during the 20 years from 2003 to 2022, through the research method of bibliometrics and through the data visualization analysis. Specific data are given as follows.

5.1. Publication Year and Number of Publications

In the WOSCC statistics, a total of 680 oscillating heat pipe literatures were published from 2003 to 2022. The number of papers published each year reflect trends in a particular field of research. As shown in Figure 16, the number of published articles in this field peaked at 65 in 2017. In the past two years, the number of published documents has fluctuated, but the overall trend is a slow rise.

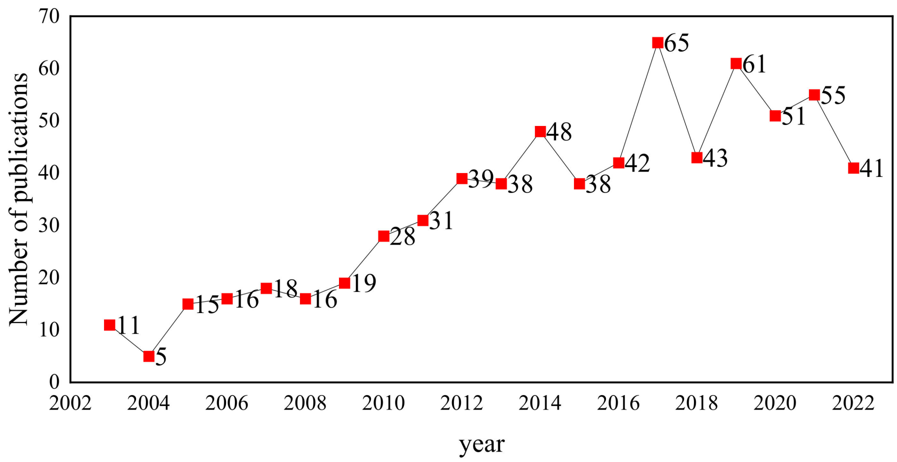

Figure 16. The growth trend of relevant literatures from 2003 to 2022.

5.2. Keyword Distribution

A keywords statistics of the above 680 literatures were carried out. A total of 41 keywords appeared more than 15 times. The top three keywords with the highest frequency are oscillating heat pipe, thermal performance, and flow, and the times are 135, 106, and 89, respectively. Figure 17 shows the connections among various words. The lines represent the number of times that these two keywords appear at the same time in a piece of literature. The thicker the lines are, the higher the number of times they appear together. The number of co-occurrences between these words is very high. Among them, the co-occurrence frequency of thermal performance and oscillating heat pipe is the highest, while the co-occurrence frequency of oscillating heat pipe and flow rank second. It can be seen that the OHP is closely related in the study of thermodynamics and fluid mechanics.

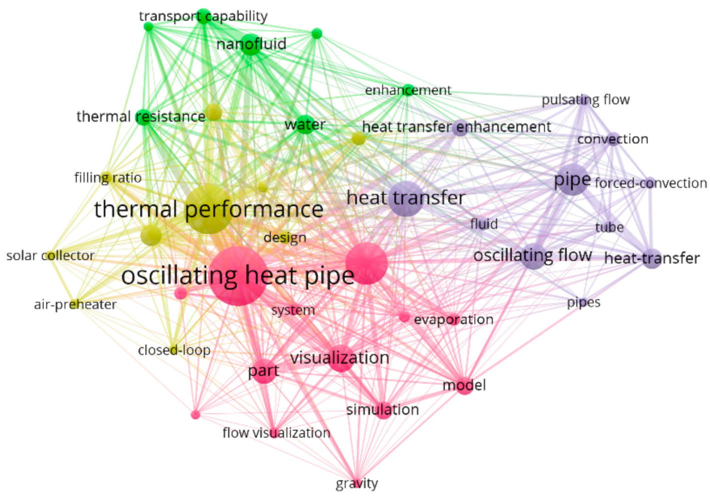

Figure 17. Analysis of each keyword.

6. Current Research Shortcomings and Prospects for Future Works

6.1. Shortcomings of the Current Studies

(1) Effects of channel layout

Studies of OHPs have focused on the effect of the fluid volume on the heat transfer performance, which neglected the synergistic effects of the layout optimization and internal flow [229].

(2) Limitation of materials

The material of the OHPs tube wall affects the heat transfer performance and the layout plasticity of the OHPs [230]. The overwhelming majority of the tube wall materials in the current study are conventional materials of copper, aluminum, and stainless steel [231,232]. The thermal conductivity of copper is relatively high, and some composite metal tube wall materials may have better performances in OHPs.

(3) Insufficient understanding of working fluid properties

The performance of the working fluid is the core material for OHPs, which directly affects the heat transfer [233]. Most of the working fluids studies have focused on water, ethanol, etc. [234,235]. For mixed nano-fluids as well as non-azeotropic mixture liquids, the effect of the concentration and mixing ratio on the optimal thermal performance of OHPs should be explored in depth. In addition, there is a lack of studies on the time-dependent properties of nano-fluid OHPs.

(4) Inadequate recognition of the heat transfer mechanism

The operation mechanism of OHPs is complex. It is not beneficial to optimize the performance of OHPs with a single thermodynamic theory to explain and derive the mechanism [236]. The interaction and influence between vapor and liquid phases have not been deeply studied, which provides a lack of accurate predictive numerical models [237].

(5) Limitations of the actual application environment

The superior heat transfer performance of OHPs should be focused on the practical use aspects. The performance of OHPs [238,239] in different use environments (e.g., rotating, centrifugal, antigravity, and horizontal) can vary significantly from operating under laboratory conditions. The actual application scenario environment will limit the operation under different working conditions [240].

6.2. Prospects for Future Research

(1) Further study of mixed nano-fluids

The nano-fluids have great potential for effective heat transfer as OHP working fluids. Through the collaborative combination of different types of nano-particles, the mixed nano-fluids can achieve higher advanced thermophysical properties and stability of single nano-fluids [241]. The influence of the mixed nano-fluid on the thermal performance of OHPs can be further studied by the optimization, analysis, and improvement of the thermal efficiency of the mixed nano-fluid [242,243].

(2) Study of non-azeotropic mixtures

Theoretical analysis shows that the non-azeotropic immiscible binary mixture can expand the operating temperature range of OHPs [244]. The non-azeotropic immiscible binary mixture can solve the problems of starting temperatures and the drying under the high heat flux of OHPs [245,246], which can improve the heat transfer performance and heat transfer limit of OHPs [247,248]. Future studies can be performed on non-azeotropic mixtures OHPs with different configurations by the analysis of the correlation among profile mixing ratio, filling ratio, and power input.

(3) The improvement in the numerical model

VOF is a widely used method in order to study the complex coupling of pressure and temperature of OHPs, which can capture the phase distribution and interface dynamics [249,250]. Lee's model is used to explain the phase transition principle. Numerical model improvements can be made to better cover the microscopic and macroscopic levels [251]. Dreiling et al. [252] proposed a closed-interface tracking CFD-VOF method. The effect of factors of the film around the bubble and the curvature of the interface, turbulence, or mass transfer strength parameters on the OHP can be systematically investigated. More stable and effective turbulence models that are applicable for OHPs need to be developed in the prospective.

(4) The combination of artificial intelligence technology

Artificial intelligence techniques, in terms of efficiency and intelligence, have also been applied in the field of OHPs [253]. Many cases of research with deep learning algorithms optimize the parameters of OHPs [254]. With the development of AI technology, the computational work of optimization algorithms has become more comfortable. Wen et al. [255] modeled acetone OHP thermal resistance with human neural networks, and the R-squared of the models proposed with MLP and GMDH were 0.989 and 0.965, which were able to predict and simulate acetone-filled OHP thermal resistance. Jokar et al. [256] proposed OHP simulation and optimization with the genetic algorithm approach and the obtained the optimum filling rate of 38.25%.

7. Conclusions

This paper describes the various filling working fluids and in-tube flow states on the heat dissipation properties of OHPs. The effect of metal nano-fluids, non-metallic nano-fluids, mixed nano-fluids, gas working fluids, organic solvents, mixed liquids, and SRWF fluids are given. The different heating methods of the evaporation section, flow state, gravity effect, flow pattern, and oscillatory characteristics of the tube are illustrated. The following are the main conclusions.

(1) With the addition of non-metallic nano-fluids in OHPs, the thermal resistance decreases from 24% to 83.6% with the change in the type, size, and concentration of nano-particles. The maximum heat pipe thermal conductivity was enhanced by 105% with the graphene nano-fluids. OHPs with gas as the working fluid can be used in the field of low temperature cooling. The effective thermal conductivity varies from 4.8 kW/(m·K) to 70 kW/(m·K) when different gases are selected as the working fluid in OHPs.

(2) Compared with the pure working fluid, the thermal resistance of OHPs can be reduced by 68.9% with the right mixture type, filling rate, and mixing ratio. The surfactant and SRWF can be added to reduce the surface tension of the working fluid and the thermal resistance of the OHP can be reduced by 4.78% to 60%.
(3) The change in gravity has a significant effect on the heat transfer performance of OHPs with vertical heating. A sensible heat transfer can account for more than 80% of the total heat transfer when the internal flow type of OHPs is the slug flow. The heat transfer performance is enhanced with the increase in the oscillatory flow, amplitude and the effective thermal conductivity can reach 40 kW/(m·K). The input power is increased from 7 W to 16 W, the oscillation amplitude is increased from 3.4 mm to 8.3 mm, and the thermal resistance is reduced by 13.5%.

Author Contributions: X.Z.: conceptualization, writing and check.; L.S.: data processing, writing and check; J.J.: editing, correction; W.D.: drawing, English proofreading; D.Z.: conceptualization, editing, and English revision. All authors have read and agreed to the published version of the manuscript.

Funding: This work is supported by the Young Scientists Fund of the National Natural Science Foundation of China under the research grant of 52106151 and Guangdong Basic and Applied Basic Research Foundation of 2023A1515011918.

Data Availability Statement: Not applicable.

Conflicts of Interest: The authors declare that they have no conflict of interests regarding the publication of this paper.

Nomenclature

R_{th}	the thermal resistance, K/W
$\overline{T}_{\text{evap}}$	the average temperature of the evaporation, K
$\overline{T}_{\text{cond}}$	the average temperature of the condensation, K
Q_{in}	the input power, W
t_a	the time interval for time averaging, s
W	the width of OHP, m
L	the length of OHP, m
T_{Si}	the temperature of the silicon substrate, K
x	the horizontal coordinate, m
t	the time, s
$Q_{w,H}$	the total heat transferred from the heating wall to the liquid film, W
$Q_{w,C}$	the total heat transferred from the liquid film to the cooling wall, W
T_w	the wall temperature, K
$T_{sur,H}$	the temperature of liquid film during heating K
$T_{sur,C}$	the temperature of cooling, respectively, K
λ_l	the thermal conductivity of the liquid, W/(m·K)
δ	the liquid film thickness, m
$c_{p,l}$	the specific heat of the liquid, J/(kg·K)
ρ_l	the density of the liquid, kg/m^3
A_{cr}	the cross-sectional area of the flow path, m^2
T_w	the temperature of the channel wall, K
T_l	the temperature of liquid plug, K
$h_{w,l}$	the heat transfer coefficient between channel wall and liquid plug, W/(m^2·K)
S	the perimeter of the liquid plug, m
T_v	the temperature of the vapor plug, K
$Q_{v,sen}$	the total amount of sensible heat, W
$Q_{v,lat}$	the total amount of latent heat, W
P_v	the pressure of vapor plug, Pa
V_v	the volume of the vapor plug, m^3

$c_{v,v}$	the specific heat at constant volume, J/(kg·K)
m_v	the mass of the vapor plug, kg
$\dot{m}$	the phase change local mass flow rate, kg/(m^3·s)
L_v	the latent heat
$c_{p,v}$	the constant pressure specific heat of vapor, J/(kg·K)
T_{sat}	the saturation temperature associated with the considered pressure, K
T_{int}	the local interface temperature, K
k_{lv}	the thermal conductivity, W/(m·K)
$\vec{N}$	the normal vector pointing in the direction of the gas phase at the Γ of the interface
γ	the adjustment factor
M	the molecular weight
R_g	the general gas constant, J/(mol·K)
ρ_v	the density of vapor, kg/m^3
T_{if}	the interface temperature, K
$\dot{m}_{lv}$	the mass transfer of each time step in the evaporation process, kg/(m^3·s)
$\dot{m}_{vl}$	the mass transfer of each time step in the condensation process, kg/(m^3·s)
α_l	the volume fraction of liquid
α_v	the volume fraction of vapor
MCOHP	Micro-channel oscillating heat pipe
OHP	Oscillating heat pipe
TS	Tube diameter
CVOHP	Oscillating heat pipe with check valves
CLOHP	Closed-loop oscillating heat pipe
FPOHP	Flat-plate oscillating heat pipe
SRWF	Self-rewetting fluid
MWCNTs	Multi walled carbon nano-tubes
EOHP	Ethane oscillating heat pipe
CTOHP	Capillary tube oscillating heat pipe
CTAC	Cetyltrimethylammonium chloride
CTAB	Cetyltrimethylammonium bromide
VOF	Volume of fluid

References

1. Zhao, D.; Guan, Y. Characterizing Modal Exponential Behaviors of Self-excited Transverse and Longitudinal Combustion Instabilities. *Phys. Fluids* **2022**, *34*, 024109. [CrossRef]
2. Zhao, D.; Ji, C. Non-orthogonality analysis of thermoacoustic system with a premixed V-shaped flame. *Energy Convers. Manag.* **2014**, *85*, 102–111.
3. Li, S.; Zhao, D.; Li, J. Combustion Instabilities in a Bifurcating Tube: Open- and Closed-loop Measurements. *AIAA J.* **2014**, *52*, 2513–2523. [CrossRef]
4. Zhao, D.; Li, J. Prediction of stability behaviors of longitudinal and circumferential eigenmodes in a choked thermoacoustic combustor. *Aerosp. Sci. Technol.* **2015**, *46*, 12–21.
5. Zhao, D.; Guan, Y.; Reinecke, A. Characterizing Hydrogen-fuelled Pulsating Combustion on Thermodynamic Properties of a Combustor. *Commun. Phys.* **2019**, *2*, 44. [CrossRef]
6. Zhao, X.; Jiaqiang, E.; Liao, G.; Zhang, F.; Chen, J.; Deng, Y. Numerical simulation study on soot continuous regeneration combustion model of diesel particulate filter under exhaust gas heavy load. *Fuel* **2021**, *290*, 119795. [CrossRef]
7. Zhao, X.; Jiaqiang, E.; Zhang, Z.; Chen, J.; Liao, G.; Zhang, F.; Leng, E.; Han, D.; Hu, W. A review on heat enhancement in thermal energy conversion and management using Field Synergy Principle. *Appl. Energy* **2020**, *257*, 113995. [CrossRef]
8. Ji, C.; Zhao, D. Two-dimensional lattice Boltzmann investigation of sound absorption of perforated orifices with different geometric shapes. *Aerosp. Sci. Technol.* **2014**, *39*, 40–47. [CrossRef]
9. Zhao, D.; Reyhanoglu, M. Feedback control of acoustic disturbance transient growth in triggering thermoacoustic instability. *J. Sound Vib.* **2014**, *333*, 3639–3656. [CrossRef]
10. Zhao, D.; Gutmark, E.; Reneicke, A. Mitigating self-excited flame pulsating and thermoacoustic oscillations using perforated liners. *Sci. Bull.* **2019**, *64*, 941–952. [CrossRef]
11. Zhao, D.; Li, S.; Yang, W.; Zhang, Z. Numerical investigation of the effect of distributed heat sources on heat-to-sound conversion in a T-shaped thermoacoustic system. *Appl. Energy* **2015**, *144*, 204–213. [CrossRef]
12. Zhang, Z.; Zhao, D.; Ni, S.; Sun, Y.Z.; Wang, B.; Chen, Y.; Li, G.; Li, S. Experimental characterizing combustion emissions and thermodynamic properties of a thermoacoustic swirl combustor. *Appl. Energy* **2019**, *235*, 463–472. [CrossRef]

13. Zhao, D. Transient growth of flow disturbances in triggering a Rijke tube combustion instability. *Combust. Flame* **2012**, *159*, 2126–2137. [CrossRef]
14. Thompson, S.M.; Ma, H.B.; Winholtz, R.A.; Wilson, C. Experimental investigation of miniature three-dimensional flat-plate oscillating heat pipe. *J. Heat Transf.* **2009**, *131*, 043210. [CrossRef]
15. Zhao, D.; Qin, J.; Zheng, L.; Cao, M. Amorphous vanadium oxide/molybdenum oxide hybrid with three-dimensional ordered hierarchically porous structure as a high-performance Li-ion battery anode. *Chem. Mater.* **2016**, *28*, 4180–4190. [CrossRef]
16. Im, Y.H.; Lee, J.Y.; Ahn, T.I.; Youn, Y.J. Operational characteristics of oscillating heat pipe charged with R-134a for heat recovery at low temperature. *Int. J. Heat Mass Transf.* **2022**, *196*, 123231. [CrossRef]
17. Charoensawan, P.; Wilaipon, P.; Seehawong, N. Flat plate solar water heater with closed-loop oscillating heat pipes. *Therm. Sci.* **2021**, *25 Pt A*, 3607–3614. [CrossRef]
18. Dehshali, M.E.; Nazari, M.A.; Shafii, M.B. Thermal performance of rotating closed-loop pulsating heat pipes: Experimental investigation and semi-empirical correlation. *Int. J. Therm. Sci.* **2018**, *123*, 14–26. [CrossRef]
19. Rittidech, S.; Sangiamsuk, S. Internal flow patterns on heat transfer performance of a closed-loop oscillating heat pipe with check valves. *Exp. Heat Transf.* **2012**, *25*, 48–57. [CrossRef]
20. Gully, P.; Bonnet, F.; Nikolayev, V.S.; Luchier, N.; Tran, T.Q. Evaluation of the vapor thermodynamic state in PHP. *Heat Pipe Sci. Technol. Int. J.* **2014**, *5*, 369–376. [CrossRef]
21. Barrak, A.S.; Saleh, A.A.M.; Naji, Z.H. An experimental study of using water, methanol, and binary fluids in oscillating heat pipe heat exchanger. *Eng. Sci. Technol. Int. J.* **2020**, *23*, 357–364. [CrossRef]
22. Shafii, M.B.; Arabnejad, S.; Saboohi, Y.; Jamshidi, H. Experimental investigation of pulsating heat pipes and a proposed correlation. *Heat Transf. Eng.* **2010**, *31*, 854–861. [CrossRef]
23. Lin, H.; Tian, P.; Luo, C.; Wang, H.; Zhang, J.; Yang, J.; Peng, H. Luminescent nanofluids of organometal halide perovskite nanocrystals in silicone oils with ultrastability. *ACS Appl. Mater. Interfaces* **2018**, *10*, 27244–27251. [CrossRef] [PubMed]
24. Senjaya, R.; Inoue, T. Bubble generation in oscillating heat pipe. *Appl. Therm. Eng.* **2013**, *60*, 251–255. [CrossRef]
25. Ando, M.; Okamoto, A.; Nagai, H. Start-up and heat transfer characteristics of oscillating heat pipe with different check valve layouts. *Appl. Therm. Eng.* **2021**, *196*, 117286. [CrossRef]
26. Wang, W.W.; Wang, L.; Cai, Y.; Yang, G.B.; Zhao, F.Y.; Liu, D.; Yu, Q.H. Thermo-hydrodynamic model and parametric optimization of a novel miniature closed oscillating heat pipe with periodic expansion-constriction condensations. *Int. J. Heat Mass Transf.* **2020**, *152*, 119460. [CrossRef]
27. Shi, W.; Chen, H.; Pan, L.; Wang, Q. Starting and running performance of a pulsating heat pipe with micro encapsulated phase change material suspension. *Appl. Therm. Eng.* **2022**, *212*, 118626. [CrossRef]
28. Lim, J.; Kim, S.J. Effect of a channel layout on the thermal performance of a flat plate micro pulsating heat pipe under the local heating condition. *Int. J. Heat Mass Transf.* **2019**, *137*, 1232–1240. [CrossRef]
29. Liu, X.; Han, X.; Wang, Z.; Hao, G.; Zhang, Z.; Chen, Y. Application of an anti-gravity oscillating heat pipe on enhancement of waste heat recovery. *Energy Convers. Manag.* **2020**, *205*, 112404. [CrossRef]
30. Hao, T.; Ma, H.; Ma, X. Experimental investigation of oscillating heat pipe with hybrid fluids of liquid metal and water. *J. Heat Transf.* **2019**, *141*, 071802. [CrossRef]
31. Schwarz, F.; Messmer, P.; Lodermeyer, A.; Danov, V.; Fleßner, C.; Becker, S.; Hellinger, R. Analysis of improved pulsating heat pipe designs for hot spot applications. *Int. J. Heat Mass Transf.* **2022**, *196*, 123294. [CrossRef]
32. Kwon, G.H.; Kim, S.J. Operational characteristics of pulsating heat pipes with a dual-diameter tube. *Int. J. Heat Mass Transf.* **2014**, *75*, 184–195. [CrossRef]
33. Liu, X.; Chen, X.; Zhang, Z.; Chen, Y. Thermal performance of a novel dual-serpentine-channel flat-plate oscillating heat pipe used for multiple heat sources and sinks. *Int. J. Heat Mass Transf.* **2020**, *161*, 120293. [CrossRef]
34. Arai, T.; Kawaji, M. Thermal performance and flow characteristics in additive manufactured polycarbonate pulsating heat pipes with Novec 7000. *Appl. Therm. Eng.* **2021**, *197*, 117273. [CrossRef]
35. Okazaki, S.; Fuke, H.; Ogawa, H. Performance of circular Oscillating Heat Pipe for highly adaptable heat transfer layout. *Appl. Therm. Eng.* **2021**, *198*, 117497. [CrossRef]
36. Kim, S.; Zhang, Y.; Choi, J. Effects of fluctuations of heating and cooling section temperatures on performance of a pulsating heat pipe. *Appl. Therm. Eng.* **2013**, *58*, 42–51. [CrossRef]
37. Barba, M.; Bruce, R.; Bouchet, F.; Bonelli, A.; Baudouy, B. Effect of the thermo-physical properties of the working fluid on the performance of a 1-m long cryogenic horizontal pulsating heat pipe. *Int. J. Heat Mass Transf.* **2022**, *187*, 122458. [CrossRef]
38. Monroe, J.G.; Ibrahim, O.T.; Thompson, S.M. Effect of harvesting module design on the thermal performance and voltage generation of a thermoelectric oscillating heat pipe. *Appl. Therm. Eng.* **2022**, *201*, 117651. [CrossRef]
39. Bastakoti, D.; Zhang, H.; Li, D.; Cai, W.; Li, F. An overview on the developing trend of pulsating heat pipe and its performance. *Appl. Therm. Eng.* **2018**, *141*, 305–332. [CrossRef]
40. Gürsel, G.; Frijns, A.J.H.; Homburg, F.G.A.; Van Steenhoven, A.A. A mass-spring-damper model of a pulsating heat pipe with a non-uniform and asymmetric filling. *Appl. Therm. Eng.* **2015**, *91*, 80–90. [CrossRef]
41. Liu, J.; Xie, G.; Sundén, B. Flow pattern and heat transfer past two tandem arranged cylinders with oscillating inlet velocity. *Appl. Therm. Eng.* **2017**, *120*, 614–625. [CrossRef]
42. Tong, B.Y.; Wong, T.N.; Ooi, K.T. Closed-loop pulsating heat pipe. *Appl. Therm. Eng.* **2001**, *21*, 1845–1862. [CrossRef]

43. Jo, J.; Kim, J.; Kim, S.J. Experimental investigations of heat transfer mechanisms of a pulsating heat pipe. *Energy Convers. Manag.* **2019**, *181*, 331–341. [CrossRef]
44. Senjaya, R.; Inoue, T. Oscillating heat pipe simulation considering bubble generation Part I: Presentation of the model and effects of a bubble generation. *Int. J. Heat Mass Transf.* **2013**, *60*, 816–824. [CrossRef]
45. Yoon, A.; Kim, S.J. A deep-learning approach for predicting oscillating motion of liquid slugs in a closed-loop pulsating heat pipe. *Int. J. Heat Mass Transf.* **2021**, *181*, 121860. [CrossRef]
46. Yu, C.; Ji, Y.; Li, Y.; Liu, Z.; Chu, L.; Kuang, H.; Wang, Z. A three-dimensional oscillating heat pipe filled with liquid metal and ammonia for high-power and high-heat-flux dissipation. *Int. J. Heat Mass Transf.* **2022**, *194*, 123096. [CrossRef]
47. Thompson, S.M.; Cheng, P.; Ma, H.B. An experimental investigation of a three-dimensional flat-plate oscillating heat pipe with staggered microchannels. *Int. J. Heat Mass Transf.* **2011**, *54*, 3951–3959. [CrossRef]
48. Ji, Y.; Wu, M.; Feng, Y.; Yu, C.; Chu, L.; Chang, C.; Li, Y.; Xiao, X.; Ma, H. An experimental investigation on the heat transfer performance of a liquid metal high-temperature oscillating heat pipe. *Int. J. Heat Mass Transf.* **2020**, *149*, 119198. [CrossRef]
49. Ji, Y.; Wu, M.; Feng, Y.; Liu, H.; Yang, X.; Li, Y.; Chang, C. Experimental study on the effects of sodium and potassium proportions on the heat transfer performance of liquid metal high-temperature oscillating heat pipes. *Int. J. Heat Mass Transf.* **2022**, *194*, 123116. [CrossRef]
50. Czajkowski, C.; Nowak, A.I.; Ochman, A.; Pietrowicz, S. Flower Shaped Oscillating Heat Pipe at the thermosyphon condition: Performance at different rotational speeds, filling ratios, and heat supplies. *Appl. Therm. Eng.* **2022**, *212*, 118540. [CrossRef]
51. Qu, J.; Wu, H.; Cheng, P. Thermal performance of an oscillating heat pipe with Al_2O_3–water nanofluids. *Int. Commun. Heat Mass Transf.* **2010**, *37*, 111–115. [CrossRef]
52. Qu, J.; Wang, Q. Experimental study on the thermal performance of vertical closed-loop oscillating heat pipes and correlation modeling. *Appl. Energy* **2013**, *112*, 1154–1160. [CrossRef]
53. Tokuda, D.; Inoue, T. Heat transport characteristics of a sodium oscillating heat pipe: Thermal performance. *Int. J. Heat Mass Transf.* **2022**, *196*, 123281. [CrossRef]
54. Zhao, J.; Qu, J.; Rao, Z. Experiment investigation on thermal performance of a large-scale oscillating heat pipe with self-rewetting fluid used for thermal energy storage. *Int. J. Heat Mass Transf.* **2017**, *108*, 760–769. [CrossRef]
55. Lin, Z.; Wang, S.; Huo, J.; Hu, Y.; Chen, J.; Zhang, W.; Lee, E. Heat transfer characteristics and LED heat sink application of aluminum plate oscillating heat pipes. *Appl. Therm. Eng.* **2011**, *31*, 2221–2229. [CrossRef]
56. Qian, N.; Fu, Y.; Zhang, Y.; Chen, J.; Xu, J. Experimental investigation of thermal performance of the oscillating heat pipe for the grinding wheel. *Int. J. Heat Mass Transf.* **2019**, *136*, 911–923. [CrossRef]
57. Monroe, J.G.; Ibrahim, O.T.; Thompson, S.M.; Shamsaei, N. Energy harvesting via fluidic agitation of a magnet within an oscillating heat pipe. *Appl. Therm. Eng.* **2018**, *129*, 884–892. [CrossRef]
58. Zhao, J.; Rao, Z.; Liu, C.; Li, Y. Experimental investigation on thermal performance of phase change material coupled with closed-loop oscillating heat pipe (PCM/CLOHP) used in thermal management. *Appl. Therm. Eng.* **2016**, *93*, 90–100. [CrossRef]
59. Qu, J.; Ke, Z.; Zuo, A.; Rao, Z. Experimental investigation on thermal performance of phase change material coupled with three-dimensional oscillating heat pipe (PCM/3D-OHP) for thermal management application. *Int. J. Heat Mass Transf.* **2019**, *129*, 773–782. [CrossRef]
60. Jin, H.; Lin, G.; Zeiny, A.; Bai, L.; Cai, J.; Wen, D. Experimental study of transparent oscillating heat pipes filled with solar absorptive nanofluids. *Int. J. Heat Mass Transf.* **2019**, *139*, 789–801. [CrossRef]
61. Alqahtani, A.A.; Edwardson, S.; Marengo, M.; Bertola, V. Performance of flat-plate, flexible polymeric pulsating heat pipes at different bending angles. *Appl. Therm. Eng.* **2022**, *216*, 118948. [CrossRef]
62. Iwata, N.; Miyazaki, Y.; Yasuda, S.; Ogawa, H. Thermal performance and flexibility evaluation of metallic micro oscillating heat pipe for thermal strap. *Appl. Therm. Eng.* **2021**, *197*, 117342. [CrossRef]
63. Wei, A.; Qu, J.; Qiu, H.; Wang, C.; Cao, G. Heat transfer characteristics of plug-in oscillating heat pipe with binary-fluid mixtures for electric vehicle battery thermal management. *Int. J. Heat Mass Transf.* **2019**, *135*, 746–760. [CrossRef]
64. Tsai, C.Y.; Chien, H.T.; Ding, P.P.; Chan, B.; Luh, T.Y.; Chen, P.H. Effect of structural character of gold nanoparticles in nanofluid on heat pipe thermal performance. *Mater. Lett.* **2004**, *58*, 1461–1465. [CrossRef]
65. Ma, H.B.; Wilson, C.; Borgmeyer, B.; Park, K.; Yu, Q.; Choi, S.U.S.; Tirumala, M. Effect of nanofluid on the heat transport capability in an oscillating heat pipe. *Appl. Phys. Lett.* **2006**, *88*, 143116. [CrossRef]
66. Kang, S.W.; Wei, W.C.; Tsai, S.H.; Huang, C.C. Experimental investigation of nanofluids on sintered heat pipe thermal performance. *Appl. Therm. Eng.* **2009**, *29*, 973–979. [CrossRef]
67. Naphon, P.; Thongkum, D.; Assadamongkol, P. Heat pipe efficiency enhancement with refrigerant–nanoparticles mixtures. *Energy Convers. Manag.* **2009**, *50*, 772–776. [CrossRef]
68. Hajian, R.; Layeghi, M.; Sani, K.A. Experimental study of nanofluid effects on the thermal performance with response time of heat pipe. *Energy Convers. Manag.* **2012**, *56*, 63–68. [CrossRef]
69. Aydın, D.Y.; Aydın, E.; Guru, M. The effects of particle mass fraction and static magnetic field on the thermal performance of NiFe2O4 nanofluid in a heat pipe. *Int. J. Therm. Sci.* **2023**, *183*, 107875. [CrossRef]
70. Wang, S.; Lin, Z.; Zhang, W.; Chen, J. Experimental study on pulsating heat pipe with functional thermal fluids. *Int. J. Heat Mass Transf.* **2009**, *52*, 5276–5279. [CrossRef]

71. Qu, J.; Wu, H. Thermal performance comparison of oscillating heat pipes with SiO_2/water and Al_2O_3/water nanofluids. *Int. J. Therm. Sci.* **2011**, *50*, 1954–1962. [CrossRef]
72. Hung, Y.H.; Teng, T.P.; Lin, B.G. Evaluation of the thermal performance of a heat pipe using alumina nanofluids. *Exp. Therm. Fluid Sci.* **2013**, *44*, 504–511. [CrossRef]
73. Goshayeshi, H.R.; Goodarzi, M.; Safaei, M.R.; Dahari, M. Experimental study on the effect of inclination angle on heat transfer enhancement of a ferrofluid in a closed loop oscillating heat pipe under magnetic field. *Exp. Therm. Fluid Sci.* **2016**, *74*, 265–270. [CrossRef]
74. Davari, H.; Goshayeshi, H.R.; Öztop, H.F.; Chaer, I. Experimental investigation of oscillating heat pipe efficiency for a novel condenser by using Fe3O4 nanofluid. *J. Therm. Anal. Calorim.* **2020**, *140*, 2605–2614. [CrossRef]
75. Goshayeshi, H.R.; Safaei, M.R.; Goodarzi, M.; Dahari, M. Particle size and type effects on heat transfer enhancement of Ferro-nanofluids in a pulsating heat pipe. *Powder Technol.* **2016**, *301*, 1218–1226. [CrossRef]
76. Kang, S.W.; Wang, Y.C.; Liu, Y.C.; Lo, H.M. Visualization and thermal resistance measurements for a magnetic nanofluid pulsating heat pipe. *Appl. Therm. Eng.* **2017**, *126*, 1044–1050. [CrossRef]
77. Karthikeyan, V.K.; Ramachandran, K.; Pillai, B.C.; Solomon, A.B. Effect of nanofluids on thermal performance of closed loop pulsating heat pipe. *Exp. Therm. Fluid Sci.* **2014**, *54*, 171–178. [CrossRef]
78. Kim, H.J.; Lee, S.H.; Kim, S.B.; Jang, S.P. The effect of nanoparticle shape on the thermal resistance of a flat-plate heat pipe using acetone-based Al_2O_3 nanofluids. *Int. J. Heat Mass Transf.* **2016**, *92*, 572–577. [CrossRef]
79. Jafarmadar, S.; Azizinia, N.; Razmara, N.; Mobadersani, F. Thermal analysis and entropy generation of pulsating heat pipes using nanofluids. *Appl. Therm. Eng.* **2016**, *103*, 356–364. [CrossRef]
80. Goshayeshi, H.R.; Chaer, I. Experimental study and flow visualization of Fe_2O_3/kerosene in glass oscillating heat pipes. *Appl. Therm. Eng.* **2016**, *103*, 1213–1218. [CrossRef]
81. Goshayeshi, H.R.; Izadi, F.; Bashirnezhad, K. Comparison of heat transfer performance on closed pulsating heat pipe for Fe_3O_4 and ɤFe_2O_3 for achieving an empirical correlation. *Phys. E Low-Dimens. Syst. Nanostructures* **2017**, *89*, 43–49. [CrossRef]
82. Gandomkar, A.; Saidi, M.H.; Shafii, M.B.; Vandadi, M.; Kalan, K. Visualization and comparative investigations of pulsating ferro-fluid heat pipe. *Appl. Therm. Eng.* **2017**, *116*, 56–65. [CrossRef]
83. Monroe, J.G.; Kumari, S.; Fairley, J.D.; Walters, K.B.; Berg, M.J.; Thompson, S.M. On the energy harvesting and heat transfer ability of a ferro-nanofluid oscillating heat pipe. *Int. J. Heat Mass Transf.* **2019**, *132*, 162–171. [CrossRef]
84. Tanshen, M.R.; Munkhbayar, B.; Nine, M.J.; Chung, H.; Jeong, H. Effect of functionalized MWCNTs/water nanofluids on thermal resistance and pressure fluctuation characteristics in oscillating heat pipe. *Int. Commun. Heat Mass Transf.* **2013**, *48*, 93–98. [CrossRef]
85. Sadeghinezhad, E.; Mehrali, M.; Rosen, M.A.; Akhiani, A.R.; Latibari, S.T.; Mehrali, M.; Metselaar, H.S.C. Experimental investigation of the effect of graphene nanofluids on heat pipe thermal performance. *Appl. Therm. Eng.* **2016**, *100*, 775–787. [CrossRef]
86. Kim, K.M.; Bang, I.C. Effects of graphene oxide nanofluids on heat pipe performance and capillary limits. *Int. J. Therm. Sci.* **2016**, *100*, 346–356. [CrossRef]
87. Wu, Q.; Xu, R.; Wang, R.; Li, Y. Effect of C60 nanofluid on the thermal performance of a flat-plate pulsating heat pipe. *Int. J. Heat Mass Transf.* **2016**, *100*, 892–898. [CrossRef]
88. Xing, M.; Yu, J.; Wang, R. Performance of a vertical closed pulsating heat pipe with hydroxylated MWNTs nanofluid. *Int. J. Heat Mass Transf.* **2017**, *112*, 81–88. [CrossRef]
89. Zhou, Y.; Cui, X.; Weng, J.; Shi, S.; Han, H.; Chen, C. Experimental investigation of the heat transfer performance of an oscillating heat pipe with graphene nanofluids. *Powder Technol.* **2018**, *332*, 371–380. [CrossRef]
90. Nazari, M.A.; Ghasempour, R.; Ahmadi, M.H.; Heydarian, G.; Shafii, M.B. Experimental investigation of graphene oxide nanofluid on heat transfer enhancement of pulsating heat pipe. *Int. J. Heat Mass Transf.* **2018**, *91*, 90–94. [CrossRef]
91. Xu, Y.; Xue, Y.; Qi, H.; Cai, W. Experimental study on heat transfer performance of pulsating heat pipes with hybrid working fluids. *Int. J. Heat Mass Transf.* **2020**, *157*, 119727. [CrossRef]
92. Zhou, Z.; Lv, Y.; Qu, J.; Sun, Q.; Grachev, D. Performance evaluation of hybrid oscillating heat pipe with carbon nanotube nanofluids for electric vehicle battery cooling. *Appl. Therm. Eng.* **2021**, *196*, 117300. [CrossRef]
93. Zhou, Y.; Yang, H.; Liu, L.; Zhang, M.; Wang, Y.; Zhang, Y.; Zhou, B. Enhancement of start-up and thermal performance in pulsating heat pipe with GO/water nanofluid. *Powder Technol.* **2021**, *384*, 414–422. [CrossRef]
94. Zhang, D.; He, Z.; Guan, J.; Tang, S.; Shen, C. Heat transfer and flow visualization of pulsating heat pipe with silica nanofluid: An experimental study. *Int. J. Heat Mass Transf.* **2021**, *183*, 122100. [CrossRef]
95. Sadeghinezhad, E.; Akhiani, A.R.; Metselaar, H.S.C.; Latibari, S.T.; Mehrali, M.; Mehrali, M. Parametric study on the thermal performance enhancement of a thermosyphon heat pipe using covalent functionalized graphene nanofluids. *Appl. Therm. Eng.* **2020**, *175*, 115385. [CrossRef]
96. Khajehpour, E.; Noghrehabadi, A.R.; Nasab, A.E.; Nabavi, S.H. Experimental investigation of the effect of nanofluids on the thermal resistance of a thermosiphon L-shape heat pipe at different angles. *Int. Commun. Heat Mass Transf.* **2020**, *113*, 104549. [CrossRef]

97. Li, Z.; Sarafraz, M.; Mazinani, A.; Moria, H.; Tlili, I.; Alkanhal, T.A.; Goodarzi, M.; Safaei, M.R. Operation analysis, response and performance evaluation of a pulsating heat pipe for low temperature heat recovery. *Energy Convers. Manag.* **2020**, *222*, 113230. [CrossRef]
98. Choi, D.; Lee, K.Y. Experimental study on confinement effect of two-phase closed thermosyphon and heat transfer enhancement using cellulose nanofluid. *Appl. Therm. Eng.* **2021**, *183*, 116247. [CrossRef]
99. Pandey, H.; Gupta, N.K. A descriptive review of the thermal transport mechanisms in mono and hybrid nanofluid-filled heat pipes and current developments. *Therm. Sci. Eng. Prog.* **2022**, *31*, 101281. [CrossRef]
100. Zufar, M.; Gunnasegaran, P.; Ng, K.C.; Mehta, H.B. Evaluation of the thermal performance of hybrid nanofluids in pulsating heat pipe. *CFD Lett.* **2019**, *11*, 13–24.
101. Zufar, M.; Gunnasegaran, P.; Kumar, H.; Ng, K. Numerical and experimental investigations of hybrid nanofluids on pulsating heat pipe performance. *Int. J. Heat Mass Transf.* **2020**, *146*, 118887. [CrossRef]
102. Moghadasi, H.; Aminian, E.; Saffari, H.; Mahjoorghani, M.; Emamifar, A. Numerical analysis on laminar forced convection improvement of hybrid nanofluid within a U-bend pipe in porous media. *Int. J. Mech. Sci.* **2020**, *179*, 105659. [CrossRef]
103. Xu, Q.; Liu, L.; Feng, J.; Qiao, L.; Yu, C.; Shi, W.; Ding, C.; Zang, Y.; Chang, C.; Xiong, Y.; et al. A comparative investigation on the effect of different nanofluids on the thermal performance of two-phase closed thermosyphon. *Int. J. Heat Mass Transf.* **2019**, *149*, 119189. [CrossRef]
104. Mukherjee, S.; Mishra, P.C.; Aljuwayhel, N.F.; Ali, N.; Chaudhuri, P. Thermo-fluidic performance of SiO_2–ZnO/water hybrid nanofluid on enhancement of heat transport in a tube: Experimental results. *Int. J. Therm. Sci.* **2022**, *182*, 107808. [CrossRef]
105. Veeramachaneni, S.; Pisipaty, S.K.; Vedula, D.R.; Solomon, A.B.; Harsha, V.S. Effect of copper–graphene hybrid nanoplatelets in a miniature loop heat pipe. *J. Therm. Anal. Calorim.* **2022**, *147*, 5985–5999. [CrossRef]
106. Sagar, K.R.; Naik, H.B.; Mehta, H.B. Numerical study of liquid nitrogen based pulsating heat pipe for cooling superconductors. *Int. J. Refrig.* **2021**, *122*, 33–46. [CrossRef]
107. Bruce, R.; Barba, M.; Bonelli, A.; Baudouy, B. Thermal performance of a meter-scale horizontal nitrogen Pulsating Heat Pipe. *Cryogenics* **2018**, *93*, 66–74. [CrossRef]
108. Li, M.; Li, L.; Xu, D. Effect of number of turns and configurations on the heat transfer performance of helium cryogenic pulsating heat pipe. *Cryogenics* **2018**, *96*, 159–165. [CrossRef]
109. Sun, X.; Li, S.; Jiao, B.; Gan, Z.; Pfotenhauer, J. Experimental study on a hydrogen closed-loop pulsating heat pipe with two turns. *Cryogenics* **2019**, *97*, 63–69. [CrossRef]
110. Liu, Y.; Deng, H.; Pfotenhauer, J.; Gan, Z. Design of a Hydrogen Pulsating Heat Pipe. *Phys. Procedia* **2015**, *67*, 551–556. [CrossRef]
111. Liang, Q.; Li, Y.; Wang, Q. Experimental investigation on the performance of a neon cryogenic oscillating heat pipe. *Cryogenics* **2017**, *84*, 7–12. [CrossRef]
112. Liang, Q.; Li, Y.; Wang, Q. Effects of filling ratio and condenser temperature on the thermal performance of a neon cryogenic oscillating heat pipe. *Cryogenics* **2018**, *89*, 102–106. [CrossRef]
113. Barba, M.; Bruce, R.; Bouchet, F.; Bonelli, A.; Baudouy, B. Effects of filling ratio of a long cryogenic Pulsating Heat Pipe. *Appl. Therm. Eng.* **2021**, *194*, 117072. [CrossRef]
114. Sun, X.; Li, S.; Wang, B.; Jiao, B.; Pfotenhauer, J.; Miller, F.; Gan, Z. Numerical study of the thermal performance of a hydrogen pulsating heat pipe. *Int. J. Therm. Sci.* **2022**, *172*, 107302. [CrossRef]
115. Li, Y.; Wang, Q.; Chen, S.; Zhao, B.; Dai, Y. Experimental investigation of the characteristics of cryogenic oscillating heat pipe. *Int. J. Heat Mass Transf.* **2014**, *79*, 713–719. [CrossRef]
116. Xu, D.; Li, L.; Liu, H. Experimental investigation on the thermal performance of helium based cryogenic pulsating heat pipe. *Exp. Therm. Fluid Sci.* **2016**, *70*, 61–68. [CrossRef]
117. Fonseca, L.D.; Miller, F.; Pfotenhauer, J. Experimental heat transfer analysis of a cryogenic nitrogen pulsating heat Pipe at various liquid fill ratios. *Appl. Therm. Eng.* **2018**, *130*, 343–353. [CrossRef]
118. Fonseca, L.D.; Pfotenhauer, J.; Miller, F. Results of a three evaporation cryogenic helium pulsating heat pipe. *Int. J. Heat Mass Transf.* **2018**, *120*, 1275–1286. [CrossRef]
119. Senjaya, R.; Inoue, T. Effects of non-condensable gas on the performance of oscillating heat pipe, part I: Theoretical study. *Appl. Therm. Eng.* **2014**, *73*, 1387–1392. [CrossRef]
120. Senjaya, R.; Inoue, T. Effects of non-condensable gas on the performance of oscillating heat pipe, part II: Experimental study. *Appl. Therm. Eng.* **2014**, *73*, 1393–1400. [CrossRef]
121. Chen, X.; Lin, Y.; Shao, S.; Wu, W. Study on heat transfer characteristics of ethane pulsating heat pipe in middle-low temperature region. *Appl. Therm. Eng.* **2019**, *152*, 697–705. [CrossRef]
122. Sarangi, R.K.; Rane, M.V. Experimental investigations for start up and maximum heat load of closed loop pulsating heat pipe. *Procedia Eng.* **2013**, *51*, 683–687. [CrossRef]
123. Han, H.; Cui, X.; Zhu, Y.; Sun, S. A comparative study of the behavior of working fluids and their properties on the performance of pulsating heat pipes (PHP). *Int. J. Therm. Sci.* **2014**, *82*, 138–147. [CrossRef]
124. Kim, B.; Li, L.; Kim, J.; Kim, D. A study on thermal performance of parallel connected pulsating heat pipe. *Appl. Therm. Eng.* **2017**, *126*, 1063–1068. [CrossRef]
125. Miura, M.; Nagasaki, T.; Ito, Y. Experimental investigation of heat transport with oscillating liquid column in pulsating heat pipe using forced oscillation system. *Int. J. Heat Mass Transf.* **2017**, *106*, 997–1004. [CrossRef]

126. Liang, Q.; Hao, T.; Wang, K.; Ma, X.; Lan, Z.; Wang, Y. Startup and transport characteristics of oscillating heat pipe using ionic liquids. *Int. Commun. Heat Mass Transf.* **2018**, *94*, 1–13. [CrossRef]
127. Patel, V.M.; Mehta, H.B. Channel wise displacement-velocity-frequency analysis in acetone charged multi-turn Closed Loop Pulsating Heat Pipe. *Energy Convers. Manag.* **2019**, *195*, 367–383. [CrossRef]
128. Wang, P.; Cui, X.; Weng, J.; Cai, Z.; Cai, R. Experimental investigation of the heat transfer performance of an oscillating heat pipe with LiCl salt solution. *Int. J. Heat Mass Transf.* **2020**, *158*, 120033. [CrossRef]
129. Mehta, K.; Mehta, N.; Patel, V. Experimental investigation of the thermal performance of closed loop flat plate oscillating heat pipe. *Exp. Heat Transf.* **2020**, *34*, 85–103. [CrossRef]
130. Wu, L.; Chen, J.; Wang, S. Experimental study on thermal performance of a pulsating heat pipe using R1233zd(E) as working fluid. *Int. Commun. Heat Mass Transf.* **2022**, *135*, 106152. [CrossRef]
131. Takawale, A.; Abraham, S.; Sielaff, A.; Mahapatra, P.S.; Pattamatta, A.; Stephan, P. A comparative study of flow regimes and thermal performance between flat plate pulsating heat pipe and capillary tube pulsating heat pipe. *Appl. Therm. Eng.* **2018**, *149*, 613–624. [CrossRef]
132. Bastakoti, D.; Zhang, H.; Cai, W.; Li, F. An experimental investigation of thermal performance of pulsating heat pipe with alcohols and surfactant solutions. *Int. J. Heat Mass Transf.* **2018**, *117*, 1032–1040. [CrossRef]
133. Cui, X.; Zhu, Y.; Li, Z.; Shun, S. Combination study of operation characteristics and heat transfer mechanism for pulsating heat pipe. *Appl. Therm. Eng.* **2014**, *65*, 394–402. [CrossRef]
134. Bae, J.; Lee, S.Y.; Kim, S.J. Numerical investigation of effect of film dynamics on fluid motion and thermal performance in pulsating heat pipes. *Energy Convers. Manag.* **2017**, *151*, 296–310. [CrossRef]
135. Sun, Q.; Qu, J.; Li, X.; Yuan, J. Experimental investigation of thermo-hydrodynamic behavior in a closed loop oscillating heat pipe. *Exp. Therm. Fluid Sci.* **2017**, *82*, 450–458. [CrossRef]
136. Mahapatra, B.N.; Das, P.K.; Sahoo, S.S. Scaling analysis and experimental investigation of pulsating loop heat pipes. *Appl. Therm. Eng.* **2016**, *108*, 358–367. [CrossRef]
137. Xue, Z.H.; Qu, W. Experimental and theoretical research on a ammonia pulsating heat pipe: New full visualization of flow pattern and operating mechanism study. *Int. J. Heat Mass Transf.* **2017**, *106*, 149–166. [CrossRef]
138. Liu, X.; Chen, Y.; Shi, M. Dynamic performance analysis on start-up of closed-loop pulsating heat pipes (CLPHPs). *Int. J. Therm. Sci.* **2013**, *65*, 224–233. [CrossRef]
139. Hao, T.; Ma, H.; Ma, X. Heat transfer performance of polytetrafluoroethylene oscillating heat pipe with water, ethanol, and acetone as working fluids. *Int. J. Heat Mass Transf.* **2018**, *131*, 109–120. [CrossRef]
140. Pachghare, P.R.; Mahalle, A.M. Effect of pure and binary fluids on closed loop pulsating heat pipe thermal performance. *Procedia Eng.* **2013**, *51*, 624–629. [CrossRef]
141. Su, Q.; Chang, S.; Song, M.; Zhao, Y.; Dang, C. An experimental study on the heat transfer performance of a loop heat pipe system with ethanol-water mixture as working fluid for aircraft anti-icing. *Int. J. Heat Mass Transf.* **2019**, *139*, 280–292. [CrossRef]
142. Zhu, Y.; Cui, X.; Han, H.; Sun, S. The study on the difference of the start-up and heat-transfer performance of the pulsating heat pipe with water−acetone mixtures. *Int. J. Heat Mass Transf.* **2014**, *77*, 834–842. [CrossRef]
143. Han, H.; Cui, X.; Zhu, Y.; Xu, T.; Sui, Y.; Sun, S. Experimental study on a closed-loop pulsating heat pipe (CLPHP) charged with water-based binary zeotropes and the corresponding pure fluids. *Energy* **2016**, *109*, 724–736. [CrossRef]
144. Shi, S.; Cui, X.; Han, H.; Weng, J.; Li, Z. A study of the heat transfer performance of a pulsating heat pipe with ethanol-based mixtures. *Appl. Therm. Eng.* **2016**, *102*, 1219–1227. [CrossRef]
145. Cui, X.; Qiu, Z.; Weng, J.; Li, Z. Heat transfer performance of closed loop pulsating heat pipes with methanol-based binary mixtures. *Exp. Therm. Fluid Sci.* **2016**, *76*, 253–263. [CrossRef]
146. Xu, R.; Zhang, C.; Chen, H.; Wu, Q.; Wang, R. Heat transfer performance of pulsating heat pipe with zeotropic immiscible binary mixtures. *Int. J. Heat Mass Transf.* **2019**, *137*, 31–41. [CrossRef]
147. Chang, G.; Li, Y.; Zhao, W.; Xu, Y. Performance investigation of flat-plate CLPHP with pure and binary working fluids for PEMFC cooling. *Int. J. Hydrogen Energy* **2021**, *46*, 30433–30441. [CrossRef]
148. Markal, B.; Varol, R. Thermal investigation and flow pattern analysis of a closed-loop pulsating heat pipe with binary mixtures. *J. Braz. Soc. Mech. Sci. Eng.* **2020**, *42*, 549. [CrossRef]
149. Markal, B.; Varol, R. Experimental investigation and force analysis of flat-plate type pulsating heat pipes having ternary mixtures. *Int. Commun. Heat Mass Transf.* **2020**, *121*, 105084. [CrossRef]
150. Markal, B.; Varol, R. Investigation of the effects of miscible and immiscible binary fluids on thermal performance of pulsating heat pipes. *Heat Mass Transf.* **2021**, *57*, 1527–1542. [CrossRef]
151. Wang, X.H.; Zheng, H.C.; Si, M.Q.; Han, X.H.; Chen, G.M. Experimental investigation of the influence of surfactant on the heat transfer performance of pulsating heat pipe. *Int. J. Heat Mass Transf.* **2015**, *83*, 586–590. [CrossRef]
152. Patel, V.M.; Mehta, H.B. Influence of working fluids on startup mechanism and thermal performance of a closed loop pulsating heat pipe. *Appl. Therm. Eng.* **2017**, *110*, 1568–1577. [CrossRef]
153. Hao, T.; Ma, X.; Lan, Z.; Li, N.; Zhao, Y.; Ma, H. Effects of hydrophilic surface on heat transfer performance and oscillating motion for an oscillating heat pipe. *Int. J. Heat Mass Transf.* **2014**, *72*, 50–65. [CrossRef]
154. Xing, M.; Wang, R.; Xu, R. Experimental study on thermal performance of a pulsating heat pipe with surfactant aqueous solution. *Int. J. Heat Mass Transf.* **2018**, *127*, 903–909. [CrossRef]

155. Wang, J.; Li, F.C. Experimental study on the characteristics of CHF and pressure fluctuations of surfactant solution flow boiling. *Int. J. Heat Mass Transf.* **2017**, *115*, 1004–1010. [CrossRef]
156. Wang, J.; Xie, J.; Liu, X. Investigation on the performance of closed-loop pulsating heat pipe with surfactant. *Appl. Therm. Eng.* **2019**, *160*, 113998. [CrossRef]
157. Bao, K.; Wang, X.; Fang, Y.; Ji, X.; Han, X.; Chen, G. Effects of the surfactant solution on the performance of the pulsating heat pipe. *Appl. Therm. Eng.* **2020**, *178*, 115678. [CrossRef]
158. Abe, Y.; Iwasaki, A.; Tanaka, K. Microgravity Experiments on Phase Change of Self-Rewetting Fluids. *Ann. N. Y. Acad. Sci.* **2004**, *1027*, 269–285. [CrossRef]
159. Singh, B.; Kumar, P. Heat transfer enhancement in pulsating heat pipe by alcohol-water based self-rewetting fluid. *Therm. Sci. Eng. Prog.* **2020**, *22*, 100809. [CrossRef]
160. Hu, Y.; Liu, T.; Li, X.; Wang, S. Heat transfer enhancement of micro oscillating heat pipes with self-rewetting fluid. *Int. J. Heat Mass Transf.* **2014**, *70*, 496–503. [CrossRef]
161. Wu, S.C. Study of self-rewetting fluid applied to loop heat pipe. *Int. J. Therm. Sci.* **2015**, *98*, 374–380. [CrossRef]
162. Su, X.; Zhang, M.; Han, W.; Guo, X. Enhancement of heat transport in oscillating heat pipe with ternary fluid. *Int. J. Heat Mass Transf.* **2015**, *87*, 258–264. [CrossRef]
163. Su, X.; Zhang, M.; Han, W.; Guo, X. Experimental study on the heat transfer performance of an oscillating heat pipe with self-rewetting nanofluid. *Int. J. Heat Mass Transf.* **2016**, *100*, 378–385. [CrossRef]
164. Savino, R.; Di Paola, R.; Cecere, A.; Fortezza, R. Self-rewetting heat transfer fluids and nanobrines for space heat pipes. *Acta Astronaut.* **2010**, *67*, 1030–1037. [CrossRef]
165. Wang, J.; Xie, J.; Liu, X. Investigation of wettability on performance of pulsating heat pipe. *Int. J. Heat Mass Transf.* **2020**, *150*, 119354. [CrossRef]
166. Lin, Z.; Wang, S.; Chen, J.; Huo, J.; Hu, Y.; Zhang, W. Experimental study on effective range of miniature oscillating heat pipes. *Appl. Therm. Eng.* **2011**, *31*, 880–886. [CrossRef]
167. Xian, H.; Xu, W.; Zhang, Y.; Du, X.; Yang, Y. Thermal characteristics and flow patterns of oscillating heat pipe with pulse heating. *Int. J. Heat Mass Transf.* **2014**, *79*, 332–341. [CrossRef]
168. Zhao, J.; Jiang, W.; Liu, C.; Rao, Z. Thermal performance enhancement of an oscillating heat pipe with external expansion structure for thermal energy recovery and storage. *Appl. Therm. Eng.* **2019**, *155*, 667–675. [CrossRef]
169. Taft, B.S.; Rhodes, M. Experimental investigation of oscillating heat pipes under direct current and pulse width modulation heating input conditions. *Appl. Therm. Eng.* **2017**, *126*, 1018–1022. [CrossRef]
170. Chu, L.; Ji, Y.; Liu, Z.; Yu, C.; Wu, Z.; Wang, Z.; Yang, Y.; Yang, X. Structure optimization of a three-dimensional coil oscillating heat pipe. *Int. J. Heat Mass Transf.* **2022**, *183*, 122229. [CrossRef]
171. Chen, X.; Chen, S.; Zhang, Z.; Sun, D.; Liu, X. Heat transfer investigation of a flat-plate oscillating heat pipe with tandem dual channels under nonuniform heating. *Int. J. Heat Mass Transf.* **2021**, *180*, 121830. [CrossRef]
172. Mangini, D.; Mameli, M.; Fioriti, D.; Filippeschi, S.; Araneo, L.; Marengo, M. Hybrid pulsating heat pipe for space applications with non-uniform heating patterns: Ground and microgravity experiments. *Appl. Therm. Eng.* **2017**, *126*, 1029–1043. [CrossRef]
173. Peng, H.; Pai, P.F.; Ma, H. Nonlinear thermomechanical finite-element modeling, analysis and characterization of multi-turn oscillating heat pipes. *Int. J. Heat Mass Transf.* **2014**, *69*, 424–437. [CrossRef]
174. Qu, J.; Zhao, J.; Rao, Z. Experimental investigation on thermal performance of multi-layers three-dimensional oscillating heat pipes. *Int. J. Heat Mass Transf.* **2017**, *115*, 810–819. [CrossRef]
175. Yasuda, Y.; Nabeshima, F.; Horiuchi, K.; Nagai, H. Visualization of the working fluid in a flat-plate pulsating heat pipe by neutron radiography. *Int. J. Heat Mass Transf.* **2022**, *185*, 122336. [CrossRef]
176. Lim, J.; Kim, S.J. A channel layout of a micro pulsating heat pipe for an excessively localized heating condition. *Appl. Therm. Eng.* **2021**, *196*, 117266. [CrossRef]
177. Jiaqiang, E.; Zhao, X.; Deng, Y.; Zhu, H. Pressure distribution and flow characteristics of closed oscillating heat pipe during the starting process at different vacuum degrees. *Appl. Therm. Eng.* **2016**, *93*, 166–173.
178. Kharangate, C.R.; Mudawar, I. Review of computational studies on boiling and condensation. *Int. J. Heat Mass Transf.* **2017**, *108*, 1164–1196. [CrossRef]
179. Tanguy, S.; Sagan, M.; Lalanne, B.; Couderc, F.; Colin, C. Benchmarks and numerical methods for the simulation of boiling flows. *J. Comput. Phys.* **2014**, *264*, 1–22. [CrossRef]
180. Magnini, M.; Pulvirenti, B.; Thome, J. Numerical investigation of hydrodynamics and heat transfer of elongated bubbles during flow boiling in a microchannel. *Int. J. Heat Mass Transf.* **2013**, *59*, 451–471. [CrossRef]
181. Barba, M.; Bruce, R.; Baudouy, B. Numerical simulation of the thermal and fluid-dynamic behavior of a cryogenic capillary tube. *Cryogenics* **2020**, *106*, 103044. [CrossRef]
182. Nuntaphan, A.; Vithayasai, S.; Vorayos, N.; Vorayos, N.; Kiatsiriroat, T. Use of oscillating heat pipe technique as extended surface in wire-on-tube heat exchanger for heat transfer enhancement. *Int. Commun. Heat Mass Transf.* **2010**, *37*, 287–292. [CrossRef]
183. Qian, N.; Wang, X.; Fu, Y.; Zhao, Z.; Xu, J.; Chen, J. Predicting heat transfer of oscillating heat pipes for machining processes based on extreme gradient boosting algorithm. *Appl. Therm. Eng.* **2020**, *164*, 114521. [CrossRef]
184. Sun, Q.; Qu, J.; Wang, Q.; Yuan, J. Operational characteristics of oscillating heat pipes under micro-gravity condition. *Int. Commun. Heat Mass Transf.* **2017**, *88*, 28–36. [CrossRef]

185. Nemati, R.; Shafii, M.B. Advanced heat transfer analysis of a U-shaped pulsating heat pipe considering evaporative liquid film trailing from its liquid slug. *Appl. Therm. Eng.* **2018**, *138*, 475–489. [CrossRef]
186. Daimaru, T.; Nagai, H.; Ando, M.; Tanaka, K.; Okamoto, A.; Sugita, H. Comparison between numerical simulation and on-orbit experiment of oscillating heat pipes. *Int. J. Heat Mass Transf.* **2017**, *109*, 791–806.
187. Adachi, T.; Fujita, K.; Nagai, H. Numerical study of temperature oscillation in loop heat pipe. *Appl. Therm. Eng.* **2019**, *163*, 114281. [CrossRef]
188. Odagiri, K.; Wolk, K.; Cappucci, S.; Morellina, S.; Roberts, S.; Pate, A.; Furst, B.; Sunada, E.; Daimaru, T. Three-dimensional heat transfer analysis of flat-plate oscillating heat pipes. *Appl. Therm. Eng.* **2021**, *195*, 117189. [CrossRef]
189. Jahan, S.A.; Ali, M.; Islam, M.Q. Effect of inclination angles on heat transfer characteristics of a closed loop pulsating heat pipe. *Procedia Eng.* **2013**, *56*, 82–87. [CrossRef]
190. Mameli, M.; Araneo, L.; Filippeschi, S.; Marelli, L.; Testa, R.; Marengo, M. Thermal response of a closed loop pulsating heat pipe under a varying gravity force. *Int. J. Therm. Sci.* **2014**, *80*, 11–22. [CrossRef]
191. Mameli, M.; Manno, V.; Filippeschi, S.; Marengo, M. Thermal instability of a Closed Loop Pulsating Heat Pipe: Combined effect of orientation and filling ratio. *Exp. Therm. Fluid Sci.* **2014**, *59*, 222–229. [CrossRef]
192. Ayel, V.; Araneo, L.; Scalambra, A.; Mameli, M.; Romestant, C.; Piteau, A.; Marengo, M.; Filippeschi, S.; Bertin, Y. Experimental study of a closed loop flat plate pulsating heat pipe under a varying gravity force. *Int. J. Therm. Sci.* **2015**, *96*, 23–34. [CrossRef]
193. Mangini, D.; Mameli, M.; Georgoulas, A.; Araneo, L.; Filippeschi, S.; Marengo, M. A pulsating heat pipe for space applications: Ground and microgravity experiments. *Int. J. Therm. Sci.* **2015**, *95*, 53–63. [CrossRef]
194. Cecere, A.; De Cristofaro, D.; Savino, R.; Ayel, V.; Sole-Agostinelli, T.; Marengo, M.; Romestant, C.; Bertin, Y. Experimental analysis of a flat plate pulsating heat pipe with self-rewetting fluids during a parabolic flight campaign. *Acta Astronaut.* **2018**, *147*, 454–461. [CrossRef]
195. Xing, M.; Wang, R.; Yu, J. The impact of gravity on the performance of pulsating heat pipe using surfactant solution. *Int. J. Heat Mass Transf.* **2020**, *151*, 119466. [CrossRef]
196. Pagliarini, L.; Cattani, L.; Bozzoli, F.; Mameli, M.; Filippeschi, S.; Rainieri, S.; Marengo, M. Thermal characterization of a multi-turn pulsating heat pipe in microgravity conditions: Statistical approach to the local wall-to-fluid heat flux. *Int. J. Heat Mass Transf.* **2021**, *169*, 120930. [CrossRef]
197. Lv, Y.; Xia, G.; Cheng, L.; Ma, D. Experimental investigation into unstable two phase flow phenomena during flow boiling in multi-microchannels. *Int. J. Therm. Sci.* **2021**, *166*, 106985. [CrossRef]
198. Yuan, D.; Qu, W.; Ma, T. Flow and heat transfer of liquid plug and neighboring vapor slugs in a pulsating heat pipe. *Int. J. Heat Mass Transf.* **2010**, *53*, 1260–1268. [CrossRef]
199. Karthikeyan, V.K.; Khandekar, S.; Pillai, B.C.; Sharma, P.K. Infrared thermography of a pulsating heat pipe: Flow regimes and multiple steady states. *Appl. Therm. Eng.* **2014**, *62*, 470–480. [CrossRef]
200. Spinato, G.; Borhani, N.; D'Entremont, B.P.; Thome, J.R. Time-strip visualization and thermo-hydrodynamics in a Closed Loop Pulsating Heat Pipe. *Appl. Therm. Eng.* **2015**, *78*, 364–372. [CrossRef]
201. Xian, H.; Xu, W.; Zhang, Y.; Du, X.; Yang, Y. Experimental investigations of dynamic fluid flow in oscillating heat pipe under pulse heating. *Appl. Therm. Eng.* **2015**, *88*, 376–383. [CrossRef]
202. Pouryoussefi, S.M.; Zhang, Y. Numerical investigation of chaotic flow in a 2D closed-loop pulsating heat pipe. *Appl. Therm. Eng.* **2016**, *98*, 617–627. [CrossRef]
203. Feldmann, D.; Wagner, C. On the influence of computational domain length on turbulence in oscillatory pipe flow. *Int. J. Heat Fluid Flow* **2016**, *61*, 229–244. [CrossRef]
204. Pouryoussefi, S.M.; Zhang, Y. Analysis of chaotic flow in a 2D multi-turn closed-loop pulsating heat pipe. *Appl. Therm. Eng.* **2017**, *126*, 1069–1076. [CrossRef]
205. Mangini, D.; Marengo, M.; Araneo, L.; Mameli, M.; Fioriti, D.; Filippeschi, S. Infrared analysis of the two phase flow in a single closed loop pulsating heat pipe. *Exp. Therm. Fluid Sci.* **2018**, *97*, 304–312. [CrossRef]
206. Xia, G.; Lv, Y.; Cheng, L.; Ma, D.; Jia, Y. Experimental study and dynamic simulation of the continuous two-phase instable boiling in multiple parallel microchannels. *Int. J. Heat Mass Transf.* **2019**, *138*, 961–984. [CrossRef]
207. Yoon, A.; Kim, S.J. Experimental and theoretical studies on oscillation frequencies of liquid slugs in micro pulsating heat pipes. *Energy Convers. Manag.* **2019**, *181*, 48–58. [CrossRef]
208. Ling, Y.Z.; Zhang, X.S.; Wang, X. Study of flow characteristics of an oscillating heat pipe. *Appl. Therm. Eng.* **2019**, *160*, 113995. [CrossRef]
209. Noh, H.Y.; Kim, S.J. Numerical simulation of pulsating heat pipes: Parametric investigation and thermal optimization. *Energy Convers. Manag.* **2020**, *203*, 112237. [CrossRef]
210. Ahmad, H.; Kim, S.K.; Jung, S.Y. Analysis of thermally driven flow behaviors for two-turn closed-loop pulsating heat pipe in ambient conditions: An experimental approach. *Int. J. Heat Mass Transf.* **2020**, *150*, 119245. [CrossRef]
211. Vo, D.T.; Kim, H.T.; Ko, J.; Bang, K.H. An experiment and three-dimensional numerical simulation of pulsating heat pipes. *Int. J. Heat Mass Transf.* **2020**, *150*, 119317. [CrossRef]
212. Schwarz, F.; Uddehal, S.R.; Lodermeyer, A.; Bagheri, E.M.; Forster-Heinlein, B.; Becker, S. Interaction of flow pattern and heat transfer in oscillating heat pipes for hot spot applications. *Appl. Therm. Eng.* **2021**, *196*, 117334. [CrossRef]

213. Rao, M.; Lefèvre, F.; Czujko, P.-C.; Khandekar, S.; Bonjour, J. Numerical and experimental investigations of thermally induced oscillating flow inside a capillary tube. *Int. J. Therm. Sci.* **2017**, *115*, 29–42. [CrossRef]
214. Yoon, A.; Kim, S.J. Characteristics of oscillating flow in a micro pulsating heat pipe: Fundamental-mode oscillation. *Int. J. Heat Mass Transf.* **2017**, *109*, 242–253. [CrossRef]
215. Spinato, G.; Borhani, N.; Thome, J.R. Understanding the self-sustained oscillating two-phase flow motion in a closed loop pulsating heat pipe. *Energy* **2015**, *90*, 889–899. [CrossRef]
216. Dilawar, M.; Pattamatta, A. A parametric study of oscillatory two-phase flows in a single turn Pulsating Heat Pipe using a non-isothermal vapor model. *Appl. Therm. Eng.* **2013**, *51*, 1328–1338. [CrossRef]
217. Kato, S.; Okuyama, K.; Ichikawa, T.; Mori, S. A single, straight-tube pulsating heat pipe (examination of a mechanism for the enhancement of heat transport). *Int. J. Heat Mass Transf.* **2013**, *64*, 254–262. [CrossRef]
218. Miura, M.; Nagasaki, T.; Ito, Y. Experimental study on heat transport induced by phase changes associated with liquid column oscillation in pulsating heat pipes. *Int. J. Heat Mass Transf.* **2019**, *133*, 652–661. [CrossRef]
219. Daimaru, T.; Yoshida, S.; Nagai, H. Study on thermal cycle in oscillating heat pipes by numerical analysis. *Appl. Therm. Eng.* **2017**, *113*, 1219–1227. [CrossRef]
220. Das, S.P.; Nikolayev, V.S.; Lefèvre, F.; Pottier, B.; Khandekar, S.; Bonjour, J. Thermally induced two-phase oscillating flow inside a capillary tube. *Int. J. Heat Mass Transf.* **2010**, *53*, 3905–3913. [CrossRef]
221. Jung, C.; Kim, S.J. Effects of oscillation amplitudes on heat transfer mechanisms of pulsating heat pipes. *Int. J. Heat Mass Transf.* **2021**, *165*, 120642. [CrossRef]
222. Sarangi, R.K.; Swain, A.; Kar, S.P.; Sekhar, P.C. Modeling for liquid plug oscillation frequency and amplitude of Pulsating heat pipe. *Mater. Today Proc.* **2022**, *49*, 372–377. [CrossRef]
223. Pai, P.F.; Peng, H.; Ma, H. Thermomechanical finite-element analysis and dynamics characterization of three-plug oscillating heat pipes. *Int. J. Heat Mass Transf.* **2013**, *64*, 623–635. [CrossRef]
224. Perna, R.; Abela, M.; Mameli, M.; Mariotti, A.; Pietrasanta, L.; Marengo, M.; Filippeschi, S. Flow characterization of a pulsating heat pipe through the wavelet analysis of pressure signals. *Appl. Therm. Eng.* **2020**, *171*, 115128. [CrossRef]
225. Recklin, V.; Pattamatta, A.; Stephan, P. Experimental investigation on the thermo-hydrodynamics of oscillatory meniscus in a capillary tube using FC-72 as working fluid. *Int. J. Multiph. Flow* **2015**, *75*, 82–87. [CrossRef]
226. Rao, M.; Lefèvre, F.; Khandekar, S.; Bonjour, J. Understanding transport mechanism of a self-sustained thermally driven oscillating two-phase system in a capillary tube. *Int. J. Heat Mass Transf.* **2013**, *65*, 451–459. [CrossRef]
227. Rao, M.; Lefèvre, F.; Khandekar, S.; Bonjour, J. Heat and mass transfer mechanisms of a self-sustained thermally driven oscillating liquid–vapour meniscus. *Int. J. Heat Mass Transf.* **2015**, *86*, 519–530. [CrossRef]
228. Fourgeaud, L.; Nikolayev, V.S.; Ercolani, E.; Duplat, J.; Gully, P. In situ investigation of liquid films in pulsating heat pipe. *Appl. Therm. Eng.* **2017**, *126*, 1023–1028. [CrossRef]
229. Jiaqiang, E.; Zhao, X.; Liu, H.; Chen, J.; Zuo, W.; Peng, Q. Field synergy analysis for enhancing heat transfer capability of a novel narrow-tube closed oscillating heat pipe. *Appl. Energy* **2016**, *175*, 218–228. [CrossRef]
230. Ando, M.; Okamoto, A.; Tanaka, K.; Maeda, M.; Sugita, H.; Daimaru, T.; Nagai, H. On-orbit demonstration of oscillating heat pipe with check valves for space application. *Appl. Therm. Eng.* **2018**, *130*, 552–560. [CrossRef]
231. Mito, T.; Natsume, K.; Yanagi, N.; Tamura, H.; Tamada, T.; Shikimachi, K.; Hirano, N.; Nagaya, S. Achievement of high heat removal characteristics of superconducting magnets with imbedded oscillating heat pipes. *IEEE Trans. Appl. Supercond.* **2011**, *21*, 2470–2473. [CrossRef]
232. Shi, W.; Li, W.; Pan, L.; Tan, X. Heat transfer properties and chaotic analysis of parallel type pulsating heat pipe. *Trans. Tianjin Univ.* **2011**, *17*, 435–439. [CrossRef]
233. Zhao, J.; Rao, Z.; Liu, C.; Li, Y. Experiment study of oscillating heat pipe and phase change materials coupled for thermal energy storage and thermal management. *Int. J. Heat Mass Transf.* **2016**, *99*, 252–260. [CrossRef]
234. Qu, J.; Wang, C.; Li, X.; Wang, H. Heat transfer performance of flexible oscillating heat pipes for electric/hybrid-electric vehicle battery thermal management. *Appl. Therm. Eng.* **2018**, *135*, 1–9. [CrossRef]
235. Zhao, J.; Jiang, W.; Rao, Z. Thermal performance investigation of an oscillating heat pipe with external expansion structure used for thermal energy recovery and storage. *Int. J. Heat Mass Transf.* **2019**, *132*, 920–928. [CrossRef]
236. Saha, N.; Das, P.K.; Sharma, P.K. Influence of process variables on the hydrodynamics and performance of a single loop pulsating heat pipe. *Int. J. Heat Mass Transf.* **2014**, *74*, 238–250. [CrossRef]
237. Senjaya, R.; Inoue, T. Oscillating heat pipe simulation considering bubble generation Part II: Effects of fitting and design parameters. *Int. J. Heat Mass Transf.* **2013**, *60*, 825–835. [CrossRef]
238. Lips, S.; Bensalem, A.; Bertin, Y.; Ayel, V.; Romestant, C.; Bonjour, J. Experimental evidences of distinct heat transfer regimes in pulsating heat pipes (PHP). *Appl. Therm. Eng.* **2010**, *30*, 900–907. [CrossRef]
239. Sun, Q.; Qu, J.; Yuan, J.; Wang, Q. Operational characteristics of an MEMS-based micro oscillating heat pipe. *Appl. Therm. Eng.* **2017**, *124*, 1269–1278. [CrossRef]
240. Nikolayev, V.S. Effect of tube heat conduction on the single branch pulsating heat pipe start-up. *Int. J. Heat Mass Transf.* **2016**, *95*, 477–487. [CrossRef]
241. Pandey, H.; Agarwal, S.; Gupta, N.K. Temporal performance evaluation of CuO + GO hybrid nanofluids in heat pipe. *Heat Transf. Res.* **2022**, *53*, 75–96. [CrossRef]

242. Abbasi, A.; Al-Khaled, K.; Khan, M.I.; Khan, S.U.; El-Refaey, A.M.; Farooq, W.; Jameel, M.; Qayyum, S. Optimized analysis and enhanced thermal efficiency of modified hybrid nanofluid (Al_2O_3, CuO, Cu) with nonlinear thermal radiation and shape features. *Case Stud. Therm. Eng.* **2021**, *28*, 101425. [CrossRef]
243. Shanmugapriya, M.; Sundareswaran, R.; Kumar, P.S. Heat and Mass Transfer Enhancement of MHD Hybrid Nanofluid Flow in the Presence of Activation Energy. *Int. J. Chem. Eng.* **2021**, *2021*, 9473226. [CrossRef]
244. Rao, Z.; Wang, Q.; Zhao, J.; Huang, C. Experimental investigation on the thermal performance of a closed oscillating heat pipe in thermal management. *Heat Mass Transf.* **2017**, *53*, 3059–3071. [CrossRef]
245. Zamani, R.; Kalan, K.; Shafii, M.B. Experimental investigation on thermal performance of closed loop pulsating heat pipes with soluble and insoluble binary working fluids and a proposed correlation. *Heat Mass Transf.* **2018**, *55*, 375–384. [CrossRef]
246. Ayel, V.; Slobodeniuk, M.; Bertossi, R.; Karmakar, A.; Martineau, F.; Romestant, C.; Bertin, Y.; Khandekar, S. Thermal performances of a flat-plate pulsating heat pipe tested with water, aqueous mixtures and surfactants. *Int. J. Therm. Sci.* **2022**, *178*, 107599. [CrossRef]
247. Rho, H.; Lee, S.; Bae, S.; Kim, T.W.; Lee, D.S.; Lee, H.J.; Hwang, J.Y.; Jeong, T.; Kim, S.; Ha, J.S.; et al. Three-Dimensional Porous Copper-Graphene Heterostructures with Durability and High Heat Dissipation Performance. *Sci. Rep.* **2015**, *5*, 12710. [CrossRef]
248. Malla, L.K.; Dhanalakota, P.; Mahapatra, P.S.; Pattamatta, A. Thermal and flow characteristics in a flat plate pulsating heat pipe with ethanol-water mixtures: From slug-plug to droplet oscillations. *Int. J. Heat Mass Transf.* **2022**, *194*, 123066. [CrossRef]
249. Li, Q.; Wang, C.; Wang, Y.; Wang, Z.; Li, H.; Lian, C. Study on the effect of the adiabatic section parameters on the performance of pulsating heat pipes. *Appl. Therm. Eng.* **2020**, *180*, 115813. [CrossRef]
250. Błasiak, P.; Opalski, M.; Parmar, P.; Czajkowski, C.; Pietrowicz, S. The Thermal—Flow Processes and Flow Pattern in a Pulsating Heat Pipe—Numerical Modelling and Experimental Validation. *Energies* **2021**, *14*, 5952. [CrossRef]
251. Zhao, J.; Wu, C.; Rao, Z. Numerical study on heat transfer enhancement of closed loop oscillating heat pipe through active incentive method. *Int. Commun. Heat Mass Transf.* **2020**, *115*, 104612. [CrossRef]
252. Dreiling, R.; Dubois, V.; Zimmermann, S.; Nguyen-Xuan, T.; Schreivogel, P.; di Mare, F. Numerical investigation of slug flow in pulsating heat pipes using an interface capturing approach. *Int. J. Heat Mass Transf.* **2022**, *199*, 123459. [CrossRef]
253. Wang, X.; Yan, Y.; Meng, X.; Chen, G. A general method to predict the performance of closed pulsating heat pipe by artificial neural network. *Appl. Therm. Eng.* **2019**, *157*, 113761. [CrossRef]
254. Jalilian, M.; Kargarsharifabad, H.; Abbasi Godarzi, A.; Ghofrani, A.; Shafii, M.B. Simulation and optimization of pulsating heat pipe flat-plate solar collectors using neural networks and genetic algorithm: A semi-experimental investigation. *Clean Technol. Environ. Policy* **2016**, *18*, 2251–2264. [CrossRef]
255. Wen, J. Thermal resistance modeling of oscillating heat pipes filled with acetone by using artificial neural network. *J. Therm. Anal. Calorim.* **2021**, *144*, 1873–1881. [CrossRef]
256. Jokar, A.; Godarzi, A.A.; Saber, M.; Shafii, M.B. Simulation and optimization of a pulsating heat pipe using artificial neural network and genetic algorithm. *Heat Mass Transf.* **2016**, *52*, 2437–2445. [CrossRef]